Development of new tools to study lipidated mammalian ATG8

Sang-Won Park
Kyungpook National University
Pureum Jeon
Hannam University
Akinori Yamasaki
Tokyo Institute of Technology https://orcid.org/0000-0002-5820-5549
Hye Eun Lee
Korea Brain Research Institute
Ji Young Mun
Korea Brain Research Institute
Yong-Woo Jun
Kyungpook National University
Ju-Hui Park
Kyungpook National University
Seung-Hwan Lee
Kyungpook National University
Soo-Kyeong Lee
Hannam University
Hyun Kyu Song
Korea University
You-Kyung Lee
Hannam University
Michael Lazarou
Monash University https://orcid.org/0000-0003-2150-5545
Dong-Hyung Cho
Graduate School of East-West Medical Science, Kyung Hee University
Masaaki Komatsu
Juntendo University https://orcid.org/0000-0001-7672-7722
Nobuo Noda
Microbial Chemistry Research Foundation https://orcid.org/0000-0002-6940-8069
Deok-Jin Jang
Kyungpook National University
Jin-A Lee (jlmaranatha@gmail.com)

Hannam University https://orcid.org/0000-0002-6757-8371

Article

Keywords: Autophagy, mammalian ATG8, LIR motif, LC3C, GABARAP-L2, GABARAP, GABARAP-L1, selective mATG8-PE delipidation, RavZ protein

Posted Date: February 16th, 2021

DOI: https://doi.org/10.21203/rs.3.rs-221701/v1

Development of new tools to study lipidated mammalian ATG8

Sang-Won Park,[1,10] Pureum Jeon,[2,10] Akinori Yamasaki,[3,4,10] Hye Eun Lee,[5] Ji Young Mun,[5] Yong-Woo Jun,[1] Ju-Hui Park,[1] Seung-Hwan Lee,[1] Soo-Kyeong Lee,[2] You-Kyung Lee,[2] Hyun Kyu Song,[6] Michael Lazarou,[7] Dong-Hyong Cho,[8] Masaaki Komatsu,[9] Nobuo N. Noda,[3,*] Deok-Jin Jang,[1,*], and Jin-A Lee[2,*]

[1]Department of Ecological Science, College of Ecology and Environment, Kyungpook National University, Sangju 37224, Korea

[2]Department of Biological Sciences and Biotechnology, College of Life Sciences and Nanotechnology, Hannam University, Daejeon 34054, Korea

[3]Institute of Microbial Chemistry (BIKAKEN), Tokyo, Japan

[4]Present address: Cell Biology Center, Institute of Innovative Research, Tokyo Institute of Technology, Yokohama 226-8503, Japan

[5]Neural circuit research group, Korea Brain Research Institute, Daegu 41062, Korea

[6]Department of Life Sciences, Korea University 02841, Seoul, Korea.

[7]Department of Biochemistry and Molecular Biology, Biomedicine Discovery Institute, Monash University, Victoria 3800, Australia

[8]School of Life Sciences, Kyungpook National University, Daegu 41566, Korea

[9]Department of Physiology, Juntendo University Graduate School of Medicine, Tokyo 113-8421, Japan.

[10]These authors contributed equally.

Lead contact
*Correspondence: leeja@hnu.kr (J-A.L.), jangdj@knu.ac.kr (D-J.J.), and nn@bikaken.or.jp (N.N.N.)

Abstract

Mammals conserve multiple mammalian ATG8 proteins (mATG8s) consisting of γ-aminobutyric acid receptor-associated protein (GABARAP) and microtubule-associated protein 1 light-chain 3 (LC3) subfamilies that tightly bind to the autophagic membranes in a lipidated form. They are crucial in selective autophagy and recruit proteins bearing LC3-interacting region (LIR) motifs. However, because limited research tools are available, information about the specific roles of each lipidated mATG8 in selective autophagy is scarce. Here, we identified LIR motifs specific to the lipidated form of each mATG8 and characterized the residues critical for their selective interaction using cell-based assays and structural analyses. Then, we used these selective LIR motifs to develop probes and irreversible deconjugases that targeted selective lipidated mATG8s in the autophagic membrane, revealing that lipidated GABARAP subfamily proteins regulate aggrephagy of amyotrophic lateral sclerosis-linked protein aggregates. Our tools will be useful in elucidating the functional significance of each mATG8 protein in autophagy research.

Keywords: Autophagy, mammalian ATG8, LIR motif, LC3C, GABARAP-L2, GABARAP, GABARAP-L1, selective mATG8-PE delipidation, RavZ protein

INTRODUCTION

Autophagy is an evolutionarily conserved cellular degradation pathway that selectively or non-selectively eliminates unwanted materials, such as damaged organelles and harmful cytosolic aggregates, to protect the cell's ability to regulate homeostasis, adapt to various stressors, differentiate during development, and prevent genomic damage[1]. Recent studies on the role of autophagy in secretion and exocytosis have expanded our understanding of its biological significance[2, 3]. Furthermore, autophagy dysfunction has been linked to several human diseases, including cancer, neurodegenerative diseases, infectious diseases, liver diseases, and cardiovascular disorders[4, 5].

The autophagy process is tightly regulated by many autophagy-related (ATG) proteins. To date, more than 40 *ATG* genes have been identified in yeast and higher eukaryotes, constituting a diverse family of genes whose products not only precisely control autophagy but also play roles in membrane trafficking and signaling pathways[1]. ATG8 is a small ubiquitin-like protein in yeast that is covalently conjugated to phosphatidylethanolamine (PE) in autophagosomes following proteolytic cleavage of its C-terminus by the cysteine protease ATG4, which is also involved in the delipidation of ATG8-PE to release ATG8 from autophagosomes. This cleavage is necessary to elongate and close the phagophore membrane. Although there is only one ATG8 protein in yeast, mammals have two subgroups: the family of microtubule-associated protein light-chain 3 (LC3) proteins (LC3A, LC3B, and LC3C) and the family of γ-aminobutyric acid receptor-associated proteins (GABARAP, GABARAP-L1, and GABARAP-L2)[6]. These proteins undergo reversible lipidation by PE conjugation to their C-terminal regions in the autophagosome. Although mammalian ATG8 protein (mATG8) conjugation is crucial for conventional autophagy processes, including autophagosome biogenesis and maturation, accumulating evidence also suggests its involvement in

nonconventional autophagy processes, such as secretory autophagy, LC3-associated phagocytosis, entosis, micropinocytosis, and LC3-associated endocytosis[7]. However, the biological relevance of mATG8 diversity in conventional and nonconventional autophagy or even in autophagy-independent pathways is largely unknown.

mATG8 proteins recruit autophagic machinery that contains LC3-interacting region (LIR) motifs to autophagosomes[8, 9]. They can also sequester selective cargos into autophagosomes via LIR motif-containing receptors or adaptors during selective autophagy[10]. Therefore, the specific roles of LC3 and GABARAP subfamily proteins are regulated by many LC3- and GABARAP-interacting proteins with LIR motifs. Many mATG8-interacting proteins contain canonical LIR motifs that have a hydrophobic LIR motif with a core consensus sequence of (W/F/Y)-X-X-(L/I/V) that binds to the W-site and L-site conserved in mATG8 proteins using the amino acids W/F/Y and L/I/V, respectively, in the consensus sequence[8, 11, 12, 13, 14]. The GABARAP-selective motif was recently proposed to have a core consensus sequence of (W/F)-(I/V)-X-V, similar to that of an LIR motif[15]. However, some mATG8-interacting proteins contain non-canonical LIR motifs that do not meet the sequence requirements for canonical LIR motifs and present different structural determinants that are involved in mATG8 interactions[16, 17]. Many LIR motifs that interact with mATG8 proteins have been extensively investigated in recent studies[9, 18, 19]. However, the selective binding mechanism remains largely unknown. Several studies have used peptide-based arrays, glutathione S transferase (GST) pull-down assays, or competitive time-resolved fluorescence resonance energy transfer to examine the binding properties of LIR motifs for mATG8[9, 18, 20, 21, 22]. Although these approaches are useful, the assays are purely *in vitro* and may reflect the binding property of LIR motifs of only non-lipidated mATG8 proteins. Thus, many *in vitro* assay results may not reflect the physiological binding properties of lipidated mATG8 proteins on the autophagic membrane in cells. Therefore, identification of the functional LIR motifs and characterization of the

determinants that result in selective binding to lipidated mATG8 proteins on the autophagic membrane in cells are crucial.

In this study, we used novel cellular assays to determine the binding properties of LIR motifs to mATG8 proteins in cells. We utilized structural analyses to identify LC3C-, GABARAP-L2-, and GABARAP/GABARAP-L1-selective LIR motifs and characterize the biochemical properties responsible for their selective binding. Furthermore, we generated a new system that selectively monitors or delipidates lipidated mATG8s in the autophagic membrane by incorporating identified selective LIR motifs into RavZ, an irreversible deconjugase for mATG8. Finally, the use of these selective probes or deconjugases for mATG8-PE revealed that the GABARAP subfamily proteins regulate cellular degradation of amyotrophic lateral sclerosis (ALS)-linked TDP25 (the 25-kDa C-terminal fragment of TDP-43) protein aggregates during aggrephagy. These data demonstrate that our newly developed tools are widely applicable to elucidating the functional significance of the lipidated form of each mATG8 protein in diverse autophagic and non-autophagic processes.

RESULTS

Characterization of Binding Properties of LIR Motifs Toward Lipidated mATG8 in Hexa mATG8-knockout HeLa (HKO) Cells.

To examine the binding properties of LIR motifs for each mATG8 and to identify selective mATG8-binding LIR motifs in cells, we first used an LIR motif tagged with monomeric red fluorescent protein (mRFP) fused to a 3xNLS sequence (LIR-mRFP-3xNLS) for a nuclear localization signal or sequence (NLS) assay in HKO cells, in which endogenous mATG8s are not expressed (see detailed information in the STAR Methods section) (Figure S1A; Figure

1A). We first examined the binding properties of an LIR motif from p62 (LIR(p62)), the first LIR motif for mATG8 proteins that was identified in the autophagic membrane [23]. Each green fluorescent protein (GFP)-mATG8(GA) protein (in which the C-terminal glycine residue was replaced with alanine to impair PE conjugation [lipidation] and affect their cellular localization) was mainly localized to the nucleus in cells expressing LIR(p62)-mRFP-3xNLS but not the LIR motif mutant LIR(p62)$_m$-mRFP-3xNLS (Figures 1B). The relative GFP fluorescence intensity ratio between the nucleus and cytosol (N/C ratio) in LIR(p62)-mRFP-3xNLS-expressing cells was significantly higher than that in LIR(p62)$_m$-mRFP-3xNLS-expressing cells for all mATG8s (Figures 1C), indicating that this LIR bound to all types of non-lipidated mATG8 in cells in an LIR-dependent manner. Consistent with the NLS assay, LIR(p62)-GFP but not LIR(p62)$_m$-GFP showed binding with all mATG8 proteins in the GST pull-down and co-immunoprecipitation (co-IP) experiments using GST-mATG8 or 3xFLAG-mATG8 proteins, respectively (Figures 1D and 1E), confirming that LIR(p62) bound to all mATG8 proteins.

To validate the binding property of the p62 LIR motif to lipidated mATG8 proteins, we expressed LIR(p62)-GFP and mRFP-mATG8 in HKO cells and quantified the relative GFP fluorescence intensity ratio between the autophagosome and cytosol (A/C ratio) of LIR(p62)-GFP (Figure 1F). Unexpectedly, LIR(p62)-GFP mostly localized to mRFP-LC3 subfamily-positive autophagic membranes compared with mRFP-GABARAP subfamily-positive autophagic membranes in HKO cells, which was greatly reduced for LIR(p62)$_m$-GFP (Figures 1G and 1H), indicating that LIR(p62)-GFP was preferentially localized to LC3 subfamily-positive autophagic membranes. These results suggested that LIR(p62) could interact with all types of non-lipidated mATG8s in the soluble condition but was targeted to the autophagic membrane, probably via preferential binding to lipidated LC3 subfamily proteins.

Our results suggested that LIR motifs might have different binding properties to non-lipidated mAtg8 in solution and lipidated mATG8 on the autophagic membrane. Therefore, we further investigated and characterized the binding properties of other LIR motifs using our two alternative assay systems: GST pull-down and NLS assays. Both assays showed that an LIR motif from TBC1D25 (LIR(TBC1D25)) or FAIM2 (LIR(FAIM2)) bound to all or none of the mATG8 proteins, respectively (Figures S1B-S1E). In contrast, both of them showed preferential localization to mRFP-LC3 subfamily-positive autophagic membranes in HKO cells (Figures S1F and S1G). Thus, our results showed that some LIR motifs had differential binding properties for non-lipidated and lipidated mATG8 proteins in cells.

Identification of Selective Lipidated mATG8-binding LIR Motifs

Since our goal was to identify selective LIR motifs for lipidated mATG8 proteins, we next examined the binding properties of various GFP-fused known LIR motifs with mRFP-mATG8 proteins in HKO cells (Table 1; Figure 2). To this end, we expressed each LIR(X)-GFP (X: the protein name from which the LIR motif originated) together with each mRFP-mATG8 and quantified the A/C ratio of each mATG8 in HKO cells upon starvation in the presence of bafilomycin A1 (BafA1).

We first identified the LIR motifs preferentially binding to GABARAP-L2 (Figures 2A and 2B). A atypical LIR motif from SpHfl1 (LIR(Sp)), which binds to Atg8 in yeast[24], was mostly localized to GABARAP-L2- and weakly localized to GABARAP- and GABARAP-L1-positive autophagic membranes (Figure 2A). Intriguingly, LIR(Sp) showed strong binding to non-lipidated GABARAP-L2 and weak binding to GABARAP-L1 in the GST pull-down assay (Figure 2B). Isothermal titration calorimetry (ITC) experiments further confirmed the strong and specific binding affinity of LIR(Sp) to GABARAP-L2; the dissociation constant (K_d) of

LIR(Sp) to GABARAP-L2 was 0.24 μM, which was 8–12 times lower than that to GABARAP (1.8 μM) and GABARAP-L1 (2.9 μM) (Figure S2A). The corresponding values for LC3 subfamily proteins could not be determined because the interactions were too weak (Figure S2A). Thus, LIR(Sp) showed preferential binding to GABARAP-L2.

Next, we identified the LIR motif that preferentially localized to GABARAP-L1-positive autophagic membranes (Figures 2C and 2D). An LIR motif from Nix/BNIP-3L (LIR(Nix)) showed no significant binding to any mATG8 (Table 1). However, a phosphomimetic mutant of Nix/BNIP-3L (LIR(Nix-p)), in which two serine resides located N-terminal to the core LIR motif were substituted by phosphomimetic E residues, showed selective localization to the GABARAP-L1-positive autophagic membrane [25] (Figure 2C). On the other hand, in the GST pull-down assay, LIR(Nix-p) interacted with all mATG8 proteins (Figure 2D). These results demonstrated that LIR(Nix-p) could bind to all non-lipidated mATG8 proteins but was selective for lipidated GABARAP-L1-positive autophagic membranes in cells.

Additionally, we identified the LIR motif that preferentially localized to GABARAP- and GABARAP-L1-positive autophagic membranes (Figures 2E and 2F). The LIR motif from the C-terminus of ATG4B (LIR(4B)) showed binding to all lipidated mATG8 proteins except for LC3C (Table 1). A previous two-dimensional peptide array scan analysis showed that the replacement of F with S/T within the core region of LIR(4B) severely impaired binding to LC3B but not to GABARAP [26]. Consistent with this report, a mutation of F to T within the core region of LIR(4B) (referred to as LIR(4B(T)), which makes this motif atypical, almost diminished binding to the LC3 subfamily but showed significant binding to non-lipidated/lipidated GABARAP and GABARAP-L1 (Figures 2E and 2F). Thus, LIR(4B(T)) showed selective binding to GABARAP and GABARAP-L1.

Finally, we identified an LIR motif that preferentially localized to LC3C-positive autophagic membranes (Figures. 2G and 2H). GFP fused to the LIR motif of TP53INP2 (LIR(TP)) bound to all lipidated mATG8 proteins (Table 1). Meanwhile, the W to T mutation within the core region of LIR(TP) (referred to as LIR(TP(T)), which makes this LIR motif atypical, induced selective binding to lipidated LC3C (Figure 2G). Our GST pull-down assay confirmed the selective binding of LIR(TP(T))-GFP to LC3C (Figure 2H). ITC experiments also demonstrated the selectivity of LIR(TP(T)) toward LC3C (Figure S2B). The K_d value of LIR(TP(T)) binding to LC3C was 26.9 μM, five times lower than that of the other mATG8 proteins (>132 μM), indicating that LIR(TP(T)) could be used as an LC3C-selective LIR motif (Figure S2B). Taken together, we successfully identified selective LIR motifs for lipidated forms of LC3C, GABARAP/-L1, GABARAP-L1, and GABARAP-L2.

Structural Basis for Selective Binding of mATG8-binding LIR Motifs

We attempted to solve the crystal structures of atypical LIRs bound to mATG8 proteins to reveal the specific mechanism of LIR interaction with mATG8 proteins at the atomic level and succeeded in determining the structure of the LIR(Sp)-GABARAP-L2 fusion protein at a resolution of 1.86 Å (Figure 3A; Table S1). The structure of the LIR(Sp)-GABARAP-L2 complex was similar to that of the LIR(Sp)-SpAtg8 complex (Figure S3A). SpHfl1 LIR consisted of an α-helix, from D391 to M404, and an N-terminal tail. The helix forms extensive hydrophobic interactions with V51, P52, I55, W62, and I63 of GABARAP-L2 using M394, L397, Y398, A401, and M404. Among these, Y398 forms the most critical interaction by deeply inserting into the L-site pocket of GABARAP-L2. In addition to the hydrophobic interactions, three acidic residues, namely, D391, E393, and E395, formed electrostatic interactions with K46, R67, and R28 in GABARAP-L2, respectively (Figure 3B)[24]. Although

most interactions were similar to those in the LIR(Sp)-SpAtg8 structure, F388 of SpHfl1 was not inserted into the W-site of GABARAP-L2. Considering that alanine substitution of F388 induced a limited decrease in the binding affinity to SpAtg8, this observation implied that the W-site binding was unimportant for SpHfl1 binding to ATG8-family proteins. We also performed a sequence alignment of mATG8 proteins (Figure S3B)[24]. Among the GABARAP-L2 residues involved in the interaction with LIR(Sp), W62 was the sole residue that was not conserved in the other mATG8 proteins (F, K, or S was also observed at this position). To assess the importance of W62 for this interaction, we performed ITC experiments using three mATG8 mutants (GABARAP-L2 W62A, GABARAP F62W, and LC3B K65W) (Figure 3E). The W62A mutation in GABARAP-L2 reduced the binding affinity with LIR(Sp), but the F62W mutation in GABARAP had the opposite effect. The K65W mutation in LC3B marginally increased this interaction. Coupled with the fact that SpAtg8, which binds strongly with SpHfl1, has a Y at position 62, these data suggested that either W or Y at position 62 was necessary, but not sufficient, for the strong binding of ATG8 family proteins with SpHfl1 LIR.

The crystal structure of the LIR(TP)-mATG8 complex has not been previously reported. We failed to crystallize the LIR(TP) mutants bound to mATG8 proteins but succeeded in crystallizing and determining the structure of the wild-type LIR(TP)-GABARAP fusion protein at a resolution of 1.75 Å (Figure 3C; Table S1). The conformation of LIR(TP) was unique compared with that of canonical LIRs, whereas W35 and I38 bound to the W-site and L-site, respectively, in a canonical manner, the region N-terminal to the core LIR sequence (residues 28–33) formed an intramolecular β-sheet with the core LIR sequence (Figure 3C, left). An intramolecular but distinct β-sheet was also observed for the RavZ LIR, with the region C-terminal to the core LIR sequence forming a β-sheet with the core LIR sequence[27]. Although the LIR(TP) peptide used for crystallization possesses six acidic residues, only one residue (E29) formed an electrostatic interaction with GABARAP (R67), suggesting that the

binding affinity was largely dependent on the core LIR motif. To address the specificity of LIR(TP(T)) to LC3C, we prepared a structural model of the LIR(TP(T))-LC3C complex by superimposing the wild-type LIR(TP)-GABARAP structure onto the LC3C-NDP52 structure (Protein Data Base ID [PDBID]: 3VVW) followed by manual model adjustment (Figure 3D) [16]. NDP52 LIR possessed a non-canonical core sequence (I^{133}-L-V-V^{136}) and showed specific interaction with LC3C, with V136 binding to the L-site, whereas I133 did not bind to the W-site. The lack of canonical interaction must be compensated by additional interactions to maintain the high binding affinity, including hydrophobic interactions between V135 and LC3C F33 and a hydrogen bond between N129 and LC3C K32. In the case of LIR(TP(T)), I37 and D33 could form hydrophobic and electrostatic interactions with LC3C F33 and K32, respectively. Additionally, E29 and E31 of LIR(TP(T)) formed electrostatic interactions with R76 and K55 of LC3C, respectively. Among these residues, K55 and R76 were strictly conserved in all mATG8 proteins, and K32 was conserved within the GABARAP subfamily, whereas F33 was unique to LC3C. These observations suggested that F33 of LC3C was responsible for its observed specificity. Consistent with this, the mutation of K32/F33 to Q/H (corresponding to LC3A or LC3B) but not Y (corresponding to the GABARAP subfamily) reduced the binding affinity of LC3C to LIR(TP(T)) (Figure S1H). We noticed that the α2 helix of the LC3 family, whose C-terminus contained K32 and F33, was located closer to the LIR-binding pocket than that of GABARAP subfamily proteins (Figure S3C, left), a feature that seemed to enable K32 and F33 of LC3C to interact with D33 and I37 of LIR(TP(T)) (Figure 3D). The distinct positioning of the α2 helix could be attributed to the type of amino acid at position 18 (using GABARAP numbering). The LC3 family possessed a V at this position, which had a larger side-chain than G (GABARAP/GABARAP-L1) and S (GABARAP-L2), resulting in a steric crush of the α2 helix with the ubiquitin fold, thereby positioning the α2 helix toward the LIR-binding site (Figure S3C, right). Consistent with this, the mutation of

V26 to G (corresponding to GABARAP and GABARAP-L1) reduced the binding of lipidated LC3C to LIR(TP(T)) (Figures S1H). Therefore, the combination of K32, F33, and the properly positioned α2 helix was likely necessary for the specific binding of LC3C to LIR(TP(T)).

Development of Probes Selectively Monitoring Lipidated mATG8 Proteins on Autophagosomes

Next, we monitored mATG8-positive autophagic membranes to study the function of each mATG8 protein in autophagy or selective autophagy using each identified selective lipidated mATG8-binding LIR motif. To this end, we replaced the LIR1/2 and LIR3 motifs within RavZ(ΔCA)-GFP (termed gProbe, g: GFP) with selective lipidated mATG8-binding LIR motifs (gProbe-X, X: the protein name, from which the LIR motif originated), as described previously [28]. Each probe, which contained two LIR motifs and an MT domain, was coexpressed with each of the mRFP-mATG8 proteins in HKO cells (Figure 4A) and quantified the A/C ratio upon starvation in the presence of chloroquine (Table S2 and Figure 4B).

Among the selective LIR motifs that we characterized, LIR(Sp) was highly selective for GABARAP-L2 (Figure 2A and 2B). Therefore, we first tested whether gProbe-Sp was selectively localized to GABARAP-L2-positive autophagic membranes. Indeed, gProbe-Sp was mostly localized to GABARAP-L2-positive autophagic membranes; however, it was less but significantly localized to other types of mATG8-positive autophagic membranes, indicating that gProbe-Sp could detect all types of mATG8-positive autophagic membranes at differential levels (Figure 4B). L397 in LIR(Sp) hydrophobically interacted with W62 in GABARAP-L2, which corresponds to F62 in GABARAP/GABARAP-L1 (Figure 3). Therefore, we considered L397 a good candidate for a mutation to generate a more selective GABARAP-L2-binding LIR motif. We replaced L397 with I (LIR(Sp(I)) to generate gProbe-

Sp(I), which was selectively localized to GABARAP-L2-positive autophagic membranes (Figure 4B), suggesting that gProbe-Sp(I) is a highly selective probe for GABARAP-L2-positive autophagic membranes in cells.

Next, we subjected gProbe-TP(T), gProbe-4B(T), and gProbe-Nix-p to our cellular assay. gProbe-TP(T) was only localized to LC3C-positive autophagic membranes, whereas gProbe-4B(T) was selectively localized to GABARAP/GABARAP-L1-positive but not to other LC3 subfamily- or GABARAP-L2-positive autophagic membranes (Figure 4B). These results indicated that gProbe-TP(T) and gProbe-4B(T) were specific probes for LC3C- or GABARAP/GABARAP-L1-positive autophagic membranes, respectively. On the other hand, Probe-Nix-p was strongly associated with GABARAP-L1-positive autophagic membranes and with other types of autophagic membranes (Table S2). Thus, further mutational analyses are necessary to identify probes that specifically detect GABARAP-L1-positive autophagic membranes.

Finally, we confirmed LC3 subfamily- or GABARAP subfamily-positive autophagic membrane targeting using previously developed gProbe-Fy or gProbe-St, respectively [28], in HKO cells (Table S2). Taken together, we developed gProbe-Sp(I), gProbe-TP(T), and gProbe-4B(T) as selective probes binding to GABARAP-L2-, LC3C-, and GABARAP/GABARAP-L1-positive autophagic membranes in cells, respectively.

To further examine whether our selective LIR-based sensors could indeed detect autophagosomes at the ultrastructural level, we performed correlative light and electron microscopy (CLEM) analysis to probe positive spots of interest in whole-cell images with fluorescence light microscopy and then zoom in for a closer look with electron microscopy. This dual examination provided valuable complementary and unique information about cellular and ultrastructural structures of endogenous mATG8-positive autophagosomes. To this end,

rProbe-Fy (GFP in gProbe-Fy replaced by mRFP, r: mRFP) and gProbe-Sp(I) were cotransfected into wild-type HeLa cells to observe whether LC3 subfamily- or GABARAP-L2-selective probes could detect the same or distinct autophagosomes. The HeLa cells were treated with rapamycin (100 nM) in the presence of BafA1 (100 nM) for 2 h to maximize visible autophagosomes. Both rProbe-Fy and gProbe-Sp(I) detected autophagosomes throughout the entire cell (Figures 4C-4G). Notably, some autophagosomes were only detected by LC3 subfamily-selective rProbe-Fy (Figure 4G). Taken together, these data suggested that our new selective LIR-based probes were useful to identify autophagosomes containing distinct mATG8 subfamilies at the cellular and ultrastructural levels.

Development of Enzymes Selectively Delipidating mATG8-PE in Autophagic Membranes

To date, due to limitations in tools that can selectively inhibit or deplete each lipidated mATG8 protein, information concerning the specific roles of the lipidated and non-lipidated forms of each mATG8 protein in autophagy and in autophagy-independent pathways is scarce. Compared with mammalian ATG4B, which hydrolyzes the amide bond linking glycine and PE, RavZ hydrolyzes the amide bond between the C-terminal glycine residue and an adjacent aromatic residue, resulting in resistance to conjugation by the host machinery[29, 30]. Therefore, to generate deconjugase to selectively remove PE from mATG8-PE in our study, we replaced LIR1/2 and LIR3 in 3xFLAG-fused catalytically active RavZ protein (Deconjugase) with LIR(Fy), LIR(St), LIR(4B(T)), LIR(TP(T)), or LIR(Sp(I)), generating Deconjugase-X: Deconjugase-Fy targeted LC3A/B, Deconjugase-St targeted the GABARAP subfamily, Deconjugase-4B(T) targeted GABARAP/GABARAP-L1, Deconjugase-TP(T) targeted LC3C, and Deconjugase-Sp(I) targeted GABARAP-L2 (Figure 5A). Then, we monitored the mATG8-positive autophagic membranes in mouse embryonic fibroblasts (MEFs) expressing

Deconjugase-X (X: Fy, St, TP(T), 4B(T), or Sp(I)) using GFP-mATG8 fluorescence. The expression of Deconjugase-Fy selectively diminished LC3A/B/C-positive autophagic membranes (Figures 5B and 5C). Likewise, the expression of Deconjugase-St, Deconjugase-TP(T), Deconjugase-4B(T), and Deconjugase-Sp(I) selectively reduced the GFP-GABARAP subfamily-positive, GFP-LC3C-positive, GFP-GABARAP/GABARAP-L1-positive, and GFP-GABARAP-L2-positive autophagic membranes, respectively.

We detected endogenous levels of lipidated mATG8 proteins in Deconjugase-X (X: Fy, St, TP(T), 4B(T), or Sp(I))-expressing HEK293T cells by western blot analysis to further determine the enzyme specificity. Since the expression level of endogenous LC3C was too low to be detected by anti-LC3C antibody, we expressed 3xFLAG-LC3C and detected this using anti-FLAG antibody. The expression of Deconjugase-Fy strongly reduced the level of lipidated LC3A/B (LC3A-II and LC3B-II) and weakly reduced that of lipidated LC3C (LC3C-II) and lipidated GABARAP (GABARAP-II) proteins, whereas Deconjugase-St showed a selective reduction of the lipidated form of GABARAP subfamily proteins, indicating their selective delipidation (Figure 5D). Additionally, Deconjugase-Sp(I) selectively reduced lipidated GABARAP-L2 (GABARAP-L2-II). On the other hand, Deconjugase-TP(T) and Deconjugase-4B(T) non-selectively reduced lipidated mATG8s (Figure S4). These results indicated that Deconjugase-Fy, Deconjugase-St, and Deconjugase-Sp(I) could be used to selectively delipidate LC3A/B, the GABARAP subfamily, or GABARAP-L1, respectively.

Finally, we examined the level of p62 or NDP52 as autophagic substrates in Deconjugase-, Deconjugase-Fy-, Deconjugase-St-, or Deconjugase-Sp(I)-expressing HEK293T cells by western blot analysis [18]. p62 and NDP52 were strongly accumulated in Deconjugase-expressing HEK293T cells, indicating that Deconjugase cleaved lipidated mATG8 and inhibited autophagic degradation (Figures 5E and 5F). The p62 level was

increased in Deconjugase-Fy, Deconjugase-St, and Deconjugase-Sp(I)-expressing cells (Figure 5E), indicating that p62 was a general autophagic substrate regulated by both LC3A/B and GABARAP subfamily proteins. On the other hand, the NDP52 level was unaffected by Deconjugase-Fy expression (Figure 5F), suggesting that GABARAP subfamily proteins but not LC3A/B regulated the autophagic degradation of NDP52.

Lipidated GABARAP Subfamily Proteins Regulate TDP25-mediated Aggrephagy

We attempted to elucidate the specific roles of mATG8 proteins in aggrephagy, a type of selective autophagy [10], using our selective mATG8 LIR-based probes and deconjugases. Although several aggregate-prone proteins play roles in many different human diseases, including neurodegenerative diseases, and may be cleared via aggrephagy, little is known about the differential roles of lipidated LC3 or GABARAP subfamily proteins in aggrephagy.

Thus, we investigated which mATG8 proteins were involved in the autophagic degradation of TDP25 aggregates. TDP25 is a pathogenic aggregate-prone 25 kDa C-terminal protein of TDP-43 that has been identified in protein inclusions in several neurodegenerative diseases, including frontotemporal dementia and ALS [31, 32]. First, we transfected Myc-TDP25 into cultured cortical neurons to verify whether Myc-TDP25 aggregates were degraded by autophagy. TDP25-positive aggregates were observed 24–48 h after transfection. When autophagy was activated with trehalose, an mTOR-independent autophagy inducer, the size of the TDP25-positive aggregates was significantly reduced, but their number was unaffected (Figure 6). However, when autophagy was inhibited by BafA1 in neurons expressing Myc-TDP25 upon autophagy induction, the size of TDP25 aggregates increased, suggesting that the reduced size of TDP25 aggregates might be due to autophagic degradation of TDP25.

Next, we investigated which mATG8 proteins were involved in aggrephagy by transfecting gProbe-Fy, gProbe-St, gProbe-4B(T), or gProbe-Sp(I) into cultured cortical neurons expressing MYC-TDP25 to detect endogenous LC3 subfamily proteins, GABARAP subfamily proteins, GABARAP/GABARAP-L1, or GABARAP-L2, respectively. The neurons were treated with trehalose in the presence of BafA1 to maximize visual autophagosomes associated with or contacting TDP25 aggregates. gProbe-Fy, gProbe-St, gProbe-4B(T), and gProbe-Sp(I) were closely localized to the TDP25 aggregates (Figure S5A and S5B). Remarkably, gProbe-St, gProbe-4B(T), and gProbe-Sp(I) were more closely localized to TDP25 aggregates compared with gProbe-Fy, indicating that GABARAP subfamily proteins were preferentially localized to TDP25-positive aggregates.

Finally, we examined the size and number of TDP25 aggregates in neurons expressing Deconjugase, Deconjugase-Fy, Deconjugase-St, or Deconjugase-Sp(I) after autophagy induction with trehalose in the presence or absence of BafA1 (100 nM, 2 h) to distinguish their differential roles in the regulation of TDP25 aggregates by aggrephagy. We found that Deconjugase expression failed to reduce the size of TDP25 aggregates (Figure 6), indicating that Deconjugase cleaved and inhibited all lipidated mATG8 proteins, leading to cellular defects in aggrephagy. Interestingly, the GABARAP subfamily and GABARAP-L2 deconjugase-expressing neurons failed to reduce the size of TDP25 aggregates compared with LC3 subfamily deconjugase-expressing neurons (Figure 6). These data indicated that the lipidated form of GABARAP subfamily proteins but not LC3 subfamily proteins regulated the degradation of TDP25 aggregates during aggrephagy.

DISCUSSION

Most binding experiments with ATG8 proteins have been performed with soluble, non-

lipidated/free mATG8 proteins. However, the cellular functions of mATG8 proteins frequently occur on the autophagic membranes in cells when mATG8 is in the lipidated form. To date, there is limited knowledge regarding the differences in binding between the non-lipidated and the lipidated forms. In this study, we used our novel cellular assays to demonstrate that lipidated and non-lipidated mATG8 proteins could possess differential binding properties for the same LIR motifs. Our cellular assay showed that LIR(p62) or LIR(FAIM2) preferentially bind to the lipidated forms of LC3 subfamily proteins rather than GABARAP subfamily proteins on autophagic membranes, although they bind to all or none of the mATG8s in the non-lipidated form, respectively (Figures 1 and S1B-S1G). It has been consistently reported that p62 binds to both LC3B and GABARAP-L2 in the cytosol but only to LC3B in autophagic membranes, whereas FAIM2 only binds to lipidated LC3B (LC3B-II) via the LIR motif using co-IP experiments in cells[33, 34]. Why then do some LIR motifs show different binding properties to mATG8 depending on its localization? It is possible that the α1 helix of mATG8s is primarily involved in these binding differences. The α1 helix of yeast Atg8 undergoes a conformational change upon lipidation[35]. Interestingly, the substitution of the N-terminal α1 helix between LC3B and GABARAP-L2 reversed the recruitment efficacy of p62 to the autophagic membrane [33]. The direction of the N-terminal α1 helix is the determinant for the open and closed conformation of GABARAP subfamily proteins[36]. Therefore, it will be of great interest to examine whether the N-terminal α1 helix of mATG8s plays key roles in the binding differences between non-lipidated and lipidated mATG8s, partially through the conformational changes between open and closed states in the case of the GABARAP subfamily. Moreover, these results raise the intriguing possibility that specific functions of lipidated or non-lipidated mATG8 proteins might be tightly and differentially regulated by their interaction with LIR domains in diverse LIR-containing proteins.

LIR-based sensors have been developed to detect endogenous LC3/GABARAP subfamily

proteins[15, 37, 38]. In this study, we improved on the previous version of LIR-based autophagosome sensors by introducing highly selective LIR motifs for LC3C, GABARAP/GABARAP-L1, or GABARAP-L2. These improved sensors can detect different sets of lipidated mATG8 proteins in cells. For example, gProbe-TP(T) detects LC3C-positive autophagic membranes in wild-type HeLa cells but not in ATG5 or ATG7 KO HeLa cells or MEF cells, in which LC3C is not expressed (Figure S1I), thereby monitoring LC3C-positive autophagic membranes in cells. Therefore, our LIR-based LC3- or GABARAP subfamily-selective sensors will likely provide novel insights into the cellular localization of these proteins on autophagic membranes at different stages during macroautophagy/selective autophagy or nonconventional autophagy associated with lipidated LC3/GABARAP subfamily proteins.

Although the specific roles of each mATG8 protein in selective autophagy are mainly unknown, it is known that ATG8 is recruited together with cargo into autophagosomal membranes via interaction with autophagy receptors to facilitate cargo degradation. Interestingly, most autophagy receptors possess an LIR motif that allows their direct binding to LC3, whereas most autophagy adaptor proteins have GABARAP-specific LIRs. Therefore, it has been proposed that LC3 subfamily proteins are essential for cargo recruitment upon selective autophagy[7]. However, in all of these studies, the specific roles of the lipidated and non-lipidated forms of each mATG8 during macroautophagy/selective autophagy could not be clearly distinguished. Many studies have used a knockdown or knockout system for ATG8 proteins or ATG8 conjugation-deficient cells to study the functions of mATG8s that lead to the depletion of both lipidated and non-lipidated mATG8 proteins or inhibit the lipidation of all mATG8 proteins. To our knowledge, this is the first report to use irreversible selective deconjugases for ATG8 proteins consisting of ATG8-selective LIR motifs and the catalytic domain of RavZ to investigate the functional significance of lipidated mATG8 proteins on

autophagy. Use of the selective deconjugases revealed that endogenous GABARAP subfamily protein-positive autophagosomes are preferentially localized to and contact TDP-25 aggregates. More importantly, GABARAP proteins, including GABARAP-L2 in autophagosomes (lipidated GABARAP proteins), regulate cellular degradation of TDP-25 aggregates in an autophagy-dependent manner (Figure 6). Lipidated LC3A/B might not be involved in the cellular degradation of TDP-25 aggregates, although some LC3A/B-positive autophagosomes associate with TDP-25 aggregates. A study using mATG8-knockout HeLa cells showed that GABARAP subfamily proteins regulate Parkin-mediated mitophagy, a form of selective autophagy, whereas LC3 subfamily proteins mediate basal autophagy[39]. Wade Harper's group investigated the crucial roles of GABARAP subfamily proteins in selective autophagy, reporting that LC3 subfamily members were not involved in all of the steps of selective autophagy[40]. These results are consistent with our data, raising the remarkable possibility that lipidated GABARAP subfamily proteins contribute to selective autophagy. Additionally, based on our cellular assay, many LIR motifs selectively bind to GABARAP subfamily proteins compared with LC3A/B (Table S1). This might be because many different LIR-containing autophagy receptors or other autophagy machinery proteins including fusion components selectively bind to GABARAP subfamily proteins to regulate selective targeting or autophagic degradation. However, further detailed cellular and molecular approaches are necessary to elucidate the exact mechanism that regulates the selective interaction of each GABARAP subfamily protein and autophagy component.

In conclusion, our LC3- and GABARAP-selective LIR-based sensors and irreversible selective deconjugases for each mATG8-PE on autophagosomes allow elucidation of the cellular localization and selective functions in conventional and nonconventional autophagy associated with these lipidated mATG8 proteins.

METHODS

DNA Constructs

The sequence encoding 3xNLS was generated by polymerase chain reaction (PCR) amplification of C1-pEGFP-NUC vectors and inserted into an N3-mRFP vector to generate N3-mRFP-3xNLS using the restriction enzyme set *Xho*1-*Not*1. All LIRs, including the mutant LIRs used in these experiments, were amplified by extension PCR without a template using primers and then inserted into N3-EGFP and N3-mRFP-3xNLS vectors using the restriction enzyme set *Hind*III-*Kpn*1. We used an extended LIR motif with 10 N-terminal amino acids and 11 C-terminal amino acids in addition to the core LIR motif sequence (W/F/Y)-X-X-(L/I/V) because N-terminal and C-terminal amino acids may also contribute to mATG8 protein binding[8, 18]. Mutagenesis of the LC3 or GABARAP subfamily was amplified by PCR using mutant primers for each LC3/GABARAP subfamily member and inserted into pcDNA3.1-EGFP vectors using the restriction enzyme set *BamH*I-*Apa*1. The region encoding RavZ or $RavZ_{C258S}$ was generated by PCR amplification of pcDNA3.1(−)-FLAG-RavZ or $RavZ_{C258S}$ vectors and inserted into the C1-3xFLAG vector to generate C1-3xFLAG-RavZ or $RavZ_{C258S}$ using the restriction enzymes *Bgl*II-*Apa*1[41]. The C1-3xFLAG-RavZ(ΔMT) (Deconjugase) construct was created by replacing the membrane-targeting domain-containing catalytic domain with the catalytic domain in the C1-3xFLAG-RavZ vector. Additionally, C1-3xFLAG-$RavZ(\Delta MT)_X$ chimeras were created by replacing the RavZ LIR motifs with the LIR motifs of another protein amplified using primers. We used GST-LC3A, GST-LC3B, GST-LC3C, GST-GABARAP, GST-GABARAP-L1, GST-GABARAP-L2, and 3xFLAG and the previously described DNA constructs GFP-LC3A, GFP-LC3B, GFP-LC3C, GFP-GABARAP, GFP-GABARAP-L1, and GFP-GABARAP-L2 [38] in this study.

Cell Culture, Transfection, Confocal Microscopy, and Drug Treatment

All cells used in the experiment were cultured in Dulbecco's modified Eagle's medium supplemented with 10% (v/v) fetal bovine serum and 1% (v/v) penicillin/streptomycin in an incubator with 5% CO_2 at 37 °C. MEF, HeLa, and HKO cells were seeded in a sticky-slide eight-well system to obtain 40%–60% confluent growth on the day of imaging. The cells were transfected with the plasmid DNA constructs using calcium phosphate or Lipofectamine 2000 (Life Technologies, Carlsbad, CA, USA) 24–26 h before imaging. The relative amount of each construct was empirically decided based on the relative expression of each construct combination. The cells were observed under an inverted Zeiss LSM-700 scanning laser confocal microscope operated with ZEN software. The laser excitation and the spectral detection windows for fluorochromes were 488 nm (508–543 nm) for GFP and 561 nm (578–649 nm) for mRFP. Appropriate GFP (500–550 nm) and mRFP (575–625 nm) emission filters were used during the sequential imaging of each fluorescent protein.

Primary cortical neuron cells were isolated from Institute of Cancer Research E16 mice. The cells were transfected with a plasmid DNA construct using Lipofectamine 2000. The neurons were incubated with trehalose (100 mM, 24 h) to activate autophagy. HEK293T cells or mouse cortical neurons were treated with BafA1 (100 nM, 4 h) or chloroquine (50 μM, 4 h) to block autophagy.

Quantitative Analysis of N/C Ratios

If an LIR motif interacts with a GFP-tagged mATG8 in the cytosol, the LIR-mRFP-3xNLS should sequester the cytosolic mATG8 in the nucleus, depending on the binding preference of

the LIR-mRFP-3xNLS protein in HKO cells, in which endogenous mATG8s are not expressed (Figure S1A). This enables the quantification of the relative GFP fluorescence intensity ratio between the nucleus and cytosol (N/C ratio) as well as the calculation of the N/C ratio in live cells (Figure 1A). To test this, we used GFP-tagged mATG8 mutants (GFP-mATG8(GA)), in which the C-terminal glycine residue was replaced with alanine to impair PE conjugation (lipidation) and affect their cellular localization, as compared with a GFP-tagged wild-type mATG8 protein localized to autophagosomes. To express the quantitative ratio of the N/C fluorescence intensities, the average value of the nuclear and vesicular fluorescence intensities was measured by averaging at least five randomly selected points in the nucleus and the cytosol in a single cell using ImageJ software. In the same manner, the quantitative N/C ratio of at least five randomly selected cells was analyzed. The obtained values were normalized to the values calculated from mRFP-3xNLS-expressing cells. All statistical data were calculated and plotted using GraphPad Prism 6. We also confirmed that the expression of mRFP-3xNLS lacking an LIR motif did not affect the N/C distribution of GFP-mATG8(GA).

Quantitative Analysis of A/C Ratios

If an LIR motif interacts with a lipidated mRFP-mATG8 on the autophagic membrane, its localization from the cytosol to the mRFP-mATG8-positive autophagic membrane in cells will be observed (Figure 1F). Therefore, if the ratio of GFP fluorescence intensity between the autophagic membrane and cytosol (A/C ratio) is compared, the relative binding affinity of an LIR motif for each expressed mRFP-mATG8 on the autophagic membrane can be determined. To calculate the ratio of autophagosome/cytosol (A/C) fluorescence intensities in data obtained from fixed HKO cells after inducing and blocking autophagy flux by treatment with rapamycin and BafA1, the average value of the autophagosome or cytosol fluorescence intensity was

obtained from at least five randomly selected points in autophagosomes or in the cytosol of a single HKO cell using ImageJ. In the same manner, the quantitative A/C ratio of at least 20 randomly selected cells per experiment was obtained from three independent experiments. All statistical data were calculated and plotted using GraphPad Prism 6.

GST Pull-down Assay

For the GST pull-down assay using HEK293T cell lysates, the cells were transfected with plasmid DNA encoding GFP constructs using calcium phosphate transfection. After transfection, the cells were washed with phosphate-buffered saline (PBS), harvested, lysed in GST pull-down buffer solution (50 mM Tris-HCl pH 7.5, 150 mM NaCl, 2 mM ethylenediaminetetraacetic acid [EDTA], 1% Triton X-100, and a protease inhibitor cocktail), and cleared by centrifugation. The cell lysates were incubated overnight with purified GST-mATG8 proteins with glutathione-conjugated agarose beads at 4 °C. The following day, the samples were washed three to five times with the same GST pull-down buffer solution at 4 °C, and the remaining supernatant was removed. The samples were resuspended in sodium dodecyl sulfate-polyacrylamide gel electrophoresis (SDS-PAGE) sample buffer, immediately boiled, and analyzed via SDS-PAGE with Coomassie brilliant blue staining.

Immunoprecipitation

For transient transfections, HEK293T cells were plated at a density of 5–7 × 10^5 cells/well in six-well plates and cultured for 24 h. The cells were transfected with plasmid DNA constructs using calcium phosphate and incubated for 24 h. For FLAG immunoprecipitation, the transfected HEK293T cells were washed with PBS, harvested, and lysed with EDTA lysis

buffer solution (1% Triton X-100, 50 mM Tris-HCl pH 7.5, 150 mM NaCl, 5 mM EDTA, and a protease inhibitor cocktail). The cell lysates were incubated overnight with 50 μl (bead volume) of mouse anti-FLAG M2 antibody-conjugated beads at 4 °C. The beads were subsequently washed three times with lysis buffer. The immunoprecipitates were eluted by adding 2 μg/ml of 3xFLAG peptides and resuspended in SDS-PAGE sample buffer, immediately boiled, and analyzed by SDS-PAGE.

Western Blot

Samples obtained from the common cell lysate and from GST pull-down assays or immunoprecipitation assays were separated via SDS-PAGE, transferred to polyvinylidene difluoride membranes, blocked using a blocking buffer (5% skimmed milk powder in TBST) for 1 h at room temperature, and incubated overnight with primary antibodies at 4 °C. After three washes, the membranes were incubated with secondary antibodies and conjugated with horseradish peroxidase (HRP) for 1 h. The signals were visualized using WesternBright ECL solution. FLAG antibodies (1:10,000), GFP antibodies (1:10,000), LC3A antibodies (1:1,000), LC3B antibodies (1:1,000), GABARAP antibodies (1:1,000), GABARAP-L1 antibodies (1:500), GABARAP-L2 antibodies (1:500), p62 antibodies (1:100,000), NDP52 antibodies (1:1,000), GAPDH antibodies (1:10,000), and β-actin antibodies (1:10,000) were used. The secondary antibodies were HRP-conjugated goat anti-mouse (1:10,000) or HRP-conjugated goat anti-rabbit (1:10,000).

Correlative Light and Electron Microscopy

CLEM was performed as previously described[42]. Briefly, HeLa cells were cultured in culture dishes to 20%–30% confluency and then transfected with mRFP-LC3A/B and EGFP-GABALAPL2 using Lipofectamine 2000. Next, the cells were treated with rapamycin (100 nM) in the presence of BafA1 (100 nM) for 2 h and then imaged under a Ti-RCP confocal light microscope. The cells were fixed with 1% glutaraldehyde and 1% paraformaldehyde in 0.1 M cacodylate solution (pH 7.0) for 2 h at 4 ℃. Then, the fixed cells were washed with 0.1 M cacodylate solution, post-fixed with 2% osmium tetroxide for 1 h at 4 °C, and stained in 0.1 mg thiocarbohydrazide in 10 ml distilled water and en bloc in 1% uranyl acetate before dehydration through a graded ethanol series. Finally, the samples were embedded using an EMBed-812 embedding kit. The embedded samples were sectioned at 60 nm using an ultramicrotome, and the sections were viewed using a Tecnai G2 transmission electron microscope at 120 kV. Confocal micrographs were produced as high-quality images using PhotoZoom Pro 8 software. Enlarged fluorescence images were fitted to the electron micrographs using the Image J BigWarp program.

Lentivirus Production

To generate lentiviruses for infection, HEK293T cells were cotransfected with pLenti-EF1a-3xFLAG-RavZ, wild-type, Fyco1, stbd1, SpHfl1(I), psPAX2, and pMD2.G using Lipofectamine 2000. The culture supernatant was collected at 48 h and 72 h after transfection and passed through a 0.45-μm filter. The viral particles were concentrated via ultracentrifugation (15,000 rpm, 3 h) and resuspended in DPBS.

Immunocytochemistry

The transfected cells were washed with PBS, fixed with 4% PFA for 10 min, and permeabilized with 0.1% Triton X-100 for 10 min. Then, they were blocked with 3% bovine serum albumin for 1 h at room temperature prior to incubation overnight with anti-Myc) or anti-FLAG antibodies at 4℃ and then with fluorescent conjugated anti-mouse secondary antibodies for 2 h at room temperature. Finally, the cells were washed three times with 1× PBS and mounted onto glass slides. The preparations were analyzed using an LSM 880 confocal laser scanning microscope.

Plasmid Constructions for Crystallization and ITC

Human TP53INP2 LIR (residues 28–40) and fission yeast Hfl1 LIR (residues 386–409) were fused to the N-terminus of human GABARAP and GABARAP-L2 with F3S/V4T and W3S/M4T mutations, respectively, for the promotion of crystallization. All genes were inserted downstream of the sequence encoding the human rhinovirus (HRV) 3C protease recognition site in the pGEX6P-1 vector, except for the Hfl1 LIR-GABARAP-L2 fusion protein, which was inserted upstream of the sequence encoding the HRV 3C protease site, following the myelin basic protein (*MBP*) gene of the pET15b-MBP vector. The plasmids were constructed using NEBuilder HiFi DNA Assembly Master Mix or an In-Fusion HD Cloning Kit.

Protein and Peptide Purification

All proteins were expressed in *E. coli* BL21 (DE3). For protein purification, the bacteria were cultured at 37 °C to an OD_{600} of 0.8–1.0 and then supplemented with IPTG at 100 μM and further incubated overnight at 16 °C. The bacterial pellets were resuspended in PBS and 5 mM EDTA and sonicated for 10 min. After centrifugation, the supernatants were recovered and

subjected to GST-accept resin. The resin was washed three times with PBS and eluted with 10 mM glutathione and 50 mM Tris at pH 8.0. The eluates were desalted with PBS using a Bio-Scale Mini Bio-Gel P-6 Desalting Column and then digested overnight with HRV 3C protease at 4 °C. Artificial glycine-proline sequences were retained at the N-terminus of the gene product, except for the Hfl1 LIR-GABARAP-L2 fusion protein, which retained artificial L-E-V-L-F-Q sequences at the C-terminus. All mutations were generated via PCR-based mutagenesis. The samples were subjected to GST-accept resin to remove the digested GST tags, and the flow-through fractions were recovered. The peptides were synthesized by Cosmo Bio. Briefly, the peptides (10 mg) were dissolved in 300 µl distilled water and ~10 µl ammonium hydrate. The proteins and peptides were purified by size-exclusion chromatography with 20 mM HEPES at pH 6.8 and 150 mM sodium chloride using a Superdex 200 prep grade column or Superdex 75 10/300 GL column.

Crystallization and Diffraction Data Collection

All crystallizations were performed at 20 °C using the sitting-drop vapor-diffusion method by mixing protein and reservoir solutions at a 1:1 volume ratio. For crystallization of TP53INP2 LIR-GABARAP fusion protein, 11.79 mg/ml protein was mixed with 10% 2-propanol, 0.1 M sodium phosphate/citric acid at pH 4.2, and 0.2 M lithium sulfate. For crystallization of SpHfl1 LIR-GABARAP-L2 fusion protein, 40.931 mg/ml protein was mixed with 8% polyethylene glycol 3000 and 0.1 M sodium citrate at pH 5.8. The crystals were soaked in cryoprotectant and frozen in liquid nitrogen. The cryoprotectants for SpHfl1 LIR-GABARAP-L2 and TP53INP2 LIR-GABARAP were prepared by supplementing each reservoir solution with 25% 2-methyl-2,4-pentanediol or 33% glycerol, respectively. The flash-cooled crystals were maintained under nitrogen gas at 178 °C during data collection. Diffraction data were collected

using an EIGER X4M detector attached to the beamline BL-1A with a wavelength of 1.1000 Å. The diffraction data were indexed, integrated, and scaled using energy-dispersive X-ray spectroscopy[43].

Structure Determination

The structures of the SpHfl1 LIR-GABARAP-L2 and TP53INP2 LIR-GABARAP fusion proteins were determined by the molecular replacement method using the Phenix program[44]. GABARAP (PDBID: 1GNU) and GABARAP-L2 (PDBID: 4CO7) structures were used as the search model. Crystallographic refinement was performed using the Phenix and Coot programs [44, 45]. All structural images were prepared with PyMOL Molecular Graphics System v2.0.

Isothermal Titration Calorimetry

ITC experiments were performed using a MicroCal iTC200 calorimeter at 25 °C with stirring at 1,000 rpm. SpHfl1 and TP53INP2 peptides were prepared at 500 μM as injection samples. LC3 family and GABARAP subfamily proteins were prepared at 50 μM as cell samples. After a test injection of 0.4 μl, titration involved 18 injections of 2 μl of injection samples at intervals of 120 s into the cell. The datasets obtained from titration of the peptides into cells filled with buffer were used as reference data to subtract the heat of dilution. MicroCal Origin 7.0 software was used for data analysis. The thermal measurement data for the first test injection of the syringe samples were removed from the analysis. The thermal titration data were fitted to a single-site binding model that was used to determine thermodynamic parameters, such as enthalpy, K_d, and stoichiometry of binding (N). When the fit was not convergent due to weak interactions, N was fixed at 1.0. The error for each parameter represented the fitting error.

Quantification and Statistical Analysis

All data were presented as mean + SEM and performed in triplicate or higher. The Kolmogorov-Smirnov normality test was performed to check the Gaussian distribution of the group. For multiple group comparison, one-way ANOVA in conjunction with the Newman–Keuls multiple comparison test or the Kruskal–Wallis test followed by a Dunn multiple comparison test was performed as a parametric or non-parametric test, respectively. Statistical analysis was accomplished using GraphPad Prism 6. P values <0.05 were considered statistically significant.

Acknowledgements

We thank Y. Ishii for her help with protein preparation. This work was supported by the Basic Research Program of the National Research Foundation (NRF-2020R1A2C2005021), the Neurological Disorder Research Program (NRF-2020M3E5D9079908), the Science Research Center Program (2020R1A5A1019023), the Bio & Medical Technology Development Program of the National Research Foundation (NRF) funded by the Ministry of Science & ICT (2017M3A9G7073521) to J.-A.L.; the National Research Foundation (grant NRF-2018R1D1A1B07048822) to D-J.J.; the JSPS KAKENHI Grant-in-Aid for Scientific Research (18H03989 and 19H05707 to N.N.N. and 17K18339 to A.Y.); JST CREST (JPMJCR20E3) to N.N.N.; the Takeda Science Foundation to N.N.N. and A.Y.; the KBRI basic research program through Korea Brain Research Institute funded by the Ministry of Science and ICT (20-BR-01-09) to J.Y.M.; and a Grant-in-Aid for Scientific Research on Innovative Areas (19H05706), a Grant-in-Aid for Scientific Research (B) (18H02611), the Japan Society for the Promotion of Science (an A3 foresight program), and the Takeda Science Foundation to M. K.

Author contributions

Molecular and cellular experiments were conducted by S-W.P., P.J., Y-W.J., J-H.P., S-H.L., S-K.L., and Y-K.L. Structural analysis and ITC experiments were performed by A.Y. and N.N.N. CLEM experiments were performed by H.E.L. and J.Y.M. J-A.L. and D-J.J. designed the molecular and cellular experiments and analyzed the data. N.N.N. designed the structural and ITC experiments and analyzed the data. H.K.S., D-H.C., M.L. and M.K. analyzed and discussed biochemical/cellular data. N.N.N., D-J.J., and J-A.L. wrote the manuscript.

REFERENCES

1. Levine B, Kroemer G. Biological Functions of Autophagy Genes: A Disease Perspective. *Cell* **176**, 11-42 (2019).

2. Ponpuak M, Mandell MA, Kimura T, Chauhan S, Cleyrat C, Deretic V. Secretory autophagy. (2015).

3. Zahoor M, Farhan H. Crosstalk of Autophagy and the Secretory Pathway and Its Role in Diseases. *Int Rev Cell Mol Biol* **337**, 153-184 (2018).

4. Dikic I, Elazar Z. Mechanism and medical implications of mammalian autophagy. *Nat Rev Mol Cell Biol* **19**, 349-364 (2018).

5. Schneider JL, Cuervo AM. Autophagy and human disease: emerging themes. *Curr Opin Genet Dev* **26**, 16-23 (2014).

6. Slobodkin MR, Elazar Z. The Atg8 family: multifunctional ubiquitin-like key regulators of autophagy. *Essays Biochem* **55**, 51-64 (2013).

7. Lystad AH, Simonsen A. Mechanisms and Pathophysiological Roles of the ATG8 Conjugation Machinery. *Cells* **8**, (2019).

8. Birgisdottir AB, Lamark T, Johansen T. The LIR motif - crucial for selective autophagy. *Journal of cell science* **126**, 3237-3247 (2013).

9. Birgisdottir AB*, et al.* Members of the autophagy class III phosphatidylinositol 3-kinase complex I interact with GABARAP and GABARAPL1 via LIR motifs. *Autophagy*, 1-23 (2019).

10. Johansen T, Lamark T. Selective Autophagy: ATG8 Family Proteins, LIR Motifs and Cargo Receptors. *Journal of molecular biology* **432**, 80-103 (2020).

11. Wild P, McEwan DG, Dikic I. The LC3 interactome at a glance. *Journal of cell science* **127**, 3-9 (2014).

12. Kalvari I*, et al.* iLIR: A web resource for prediction of Atg8-family interacting proteins. *Autophagy* **10**, 913-925 (2014).

13. Ichimura Y*, et al.* Structural basis for sorting mechanism of p62 in selective autophagy. *The Journal of biological chemistry* **283**, 22847-22857 (2008).

14. Noda NN, Ohsumi Y, Inagaki F. Atg8-family interacting motif crucial for selective

autophagy. *FEBS Lett* **584**, 1379-1385 (2010).

15. Stolz A*, et al.* Fluorescence-based ATG8 sensors monitor localization and function of LC3/GABARAP proteins. *The EMBO journal* **36**, 549-564 (2017).

16. von Muhlinen N*, et al.* LC3C, bound selectively by a noncanonical LIR motif in NDP52, is required for antibacterial autophagy. *Molecular cell* **48**, 329-342 (2012).

17. Tumbarello DA*, et al.* The Autophagy Receptor TAX1BP1 and the Molecular Motor Myosin VI Are Required for Clearance of Salmonella Typhimurium by Autophagy. *PLoS pathogens* **11**, e1005174 (2015).

18. Wirth M*, et al.* Molecular determinants regulating selective binding of autophagy adapters and receptors to ATG8 proteins. *Nature communications* **10**, 2055 (2019).

19. Jatana N, Ascher DB. Human LC3 and GABARAP subfamily members achieve functional specificity via specific structural modulations. 1-17 (2019).

20. Rogov VV*, et al.* Structural and functional analysis of the GABARAP interaction motif (GIM). **18**, 1382-1396 (2017).

21. Rasmussen MS, Birgisdottir AB, Johansen T. Use of Peptide Arrays for Identification and Characterization of LIR Motifs. *Methods Mol Biol* **1880**, 149-161 (2019).

22. Johansen T*, et al.* Methods for Studying Interactions Between Atg8/LC3/GABARAP and LIR-Containing Proteins. *Methods Enzymol* **587**, 143-169 (2017).

23. Pankiv S*, et al.* p62/SQSTM1 binds directly to Atg8/LC3 to facilitate degradation of ubiquitinated protein aggregates by autophagy. *The Journal of biological chemistry* **282**, 24131-24145 (2007).

24. Liu XM, Yamasaki A, Du XM, Coffman VC, Ohsumi Y, Nakatogawa H. Lipidation-independent vacuolar functions of Atg8 rely on its noncanonical interaction with a vacuole membrane protein. **7**, (2018).

25. Rogov VV*, et al.* Phosphorylation of the mitochondrial autophagy receptor Nix enhances its interaction with LC3 proteins. **7**, 1131 (2017).

26. Skytte Rasmussen M*, et al.* ATG4B contains a C-terminal LIR motif important for binding and efficient cleavage of mammalian orthologs of yeast Atg8. *Autophagy* **13**, 834-853 (2017).

27. Kwon DH*, et al.* A novel conformation of the LC3-interacting region motif revealed by the structure of a complex between LC3B and RavZ. *Biochemical and biophysical research communications* **490**, 1093-1099 (2017).

28. Park SW*, et al.* Monitoring LC3- or GABARAP-positive autophagic membranes using modified RavZ-based probes. *Sci Rep* **9**, 16593 (2019).

29. Choy A*, et al.* The Legionella effector RavZ inhibits host autophagy through irreversible Atg8 deconjugation. *Science (New York, NY)* **338**, 1072-1076 (2012).

30. Horenkamp FA*, et al.* The Legionella Anti-autophagy Effector RavZ Targets the Autophagosome via PI3P- and Curvature-Sensing Motifs. *Dev Cell* **34**, 569-576 (2015).

31. Neumann M*, et al.* Ubiquitinated TDP-43 in frontotemporal lobar degeneration and amyotrophic lateral sclerosis. *Science (New York, NY)* **314**, 130-133 (2006).

32. Hergesheimer RC*, et al.* The debated toxic role of aggregated TDP-43 in amyotrophic lateral sclerosis: a resolution in sight? *Brain* **142**, 1176-1194 (2019).

33. Shvets E, Abada A, Weidberg H, Elazar Z. Dissecting the involvement of LC3B and GATE-16 in p62 recruitment into autophagosomes. *Autophagy* **7**, 683-688 (2011).

34. Hong CJ*, et al.* Fas-apoptotic inhibitory molecule 2 localizes to the lysosome and facilitates autophagosome-lysosome fusion through the LC3 interaction region motif-dependent interaction with LC3. *FASEB journal : official publication of the Federation of American Societies for Experimental Biology* **34**, 161-179 (2020).

35. Ichimura Y, Imamura Y, Emoto K, Umeda M, Noda T, Ohsumi Y. In vivo and in vitro reconstitution of Atg8 conjugation essential for autophagy. *The Journal of biological chemistry* **279**, 40584-40592 (2004).

36. Coyle JE, Qamar S, Rajashankar KR, Nikolov DB. Structure of GABARAP in two conformations: implications for GABA(A) receptor localization and tubulin binding. *Neuron* **33**, 63-74 (2002).

37. Jeon P, Park JH, Jun YW, Lee YK, Jang DJ, Lee JA. Development of GABARAP family protein-sensitive LIR-based probes for neuronal autophagy. *Molecular brain* **12**, 33 (2019).

38. Lee YK*, et al.* Development of LC3/GABARAP sensors containing a LIR and a hydrophobic domain to monitor autophagy. *The EMBO journal* **36**, 1100-1116 (2017).

39. Nguyen TN, Padman BS, Usher J, Oorschot V, Ramm G, Lazarou M. Atg8 family LC3/GABARAP proteins are crucial for autophagosome-lysosome fusion but not autophagosome formation during PINK1/Parkin mitophagy and starvation. *J Cell Biol* **215**, 857-874 (2016).

40. Vaites LP, Paulo JA, Huttlin EL, Harper JW. Systematic Analysis of Human Cells Lacking ATG8 Proteins Uncovers Roles for GABARAPs and the CCZ1/MON1 Regulator C18orf8/RMC1 in Macroautophagic and Selective Autophagic Flux. *Molecular and cellular biology* **38**, (2018).

41. Kwon DH*, et al.* The 1:2 complex between RavZ and LC3 reveals a mechanism for deconjugation of LC3 on the phagophore membrane. *Autophagy* **13**, 70-81 (2017).

42. Reddick LE, Alto NM. Correlative light and electron microscopy (CLEM) as a tool to visualize microinjected molecules and their eukaryotic sub-cellular targets. *Journal of visualized experiments : JoVE*, e3650 (2012).

43. Kabsch W. XDS. *Acta crystallographica Section D, Biological crystallography* **66**, 125-132 (2010).

44. Adams PD*, et al.* PHENIX: a comprehensive Python-based system for macromolecular structure solution. *Acta crystallographica Section D, Biological crystallography* **66**, 213-221 (2010).

45. Emsley P, Lohkamp B, Scott WG, Cowtan K. Features and development of Coot. *Acta crystallographica Section D, Biological crystallography* **66**, 486-501 (2010).

Figure Legends

Figure 1. Development of new methods to detect the binding affinities of LIR motifs for non-lipidated or lipidated mATG8 proteins *in vivo*. **a**, Schematic model of the detection of binding affinities of LIR motifs toward non-lipidated mATG8 proteins in HKO cells using LIR(x)-mRFP-3xNLS and GFP-mATG8(GA) constructs. LIR: LC3-interacting region motif, NLS: nuclear localization signal or sequence, mATG8: mammalian ATG8. (**b-c**) The LIR motif from p62 (LIR(p62)) interacts with all non-lipidated mATG8 proteins. ***b***, Cellular localization of LIR(p62)-mRFP-3xNLS or LIR(p62)$_m$-mRFP-3xNLS LIR motif mutants, in which some amino acids in the consensus sequence of LIR(p62) were mutated to alanine in HKO cells. **c**, Quantification of the nuclear and cytosolic (N/C) ratio of GFP fluorescence. Values are presented as means + SEM ($n \geq 20$ for each group). (**d-e**) Glutathione S transferase (GST) pull-down assays (**d**) and 3xFLAG co-immunoprecipitation (co-IP) experiments (**e**) to analyze the binding of LIR(p62)-GFP and LIR(p62)$_m$-GFP. The coprecipitated LIR(62)-GFP proteins (upper panel) were analyzed by western blot (WB) using the indicated anti-GFP antibodies. The immobilized GST fusion proteins used are displayed on Coomassie brilliant blue-stained gels (lower panel). Data from one representative experiment of three independent experiments is presented. **f**, Schematic model of the detection of binding affinities of LIR motifs toward lipidated mATG8 proteins in HKO cells using LIR(x)-GFP and mRFP-mATG8 constructs. (**g-h**) The LIR motif from p62 (LIR(p62)) interacts with lipidated LC3 subfamily proteins. **g**, Cellular localization of LIR(p62)- or LIR(p62)$_m$-GFP and each mRFP-mATG8 in HKO cells. Scale bar: 10 μm. **h**, Quantification of the autophagosome and cytosol (A/C) ratio of GFP fluorescence. Values are presented as means + SEM ($n \geq 20$ for each group). ***P < 0.001. Scale bar: 10 μm. LC3A(GA), GFP-LC3A(GA); LC3B(GA), GFP-LC3B(GA); LC3C(GA), GFP-LC3C(GA); RAP(GA), GFP-GABARAP(GA); RAP-L1(GA), GFP-GABARAP-L1(GA); RAP-L2(GA), GFP-GABARAP-L2(GA); LC3A, mRFP-LC3A; LC3B, mRFP-LC3B;

LC3C, mRFP-LC3C; RAP, mRFP-GABARAP; RAP-L1, mRFP-GABARAP-L1; RAP-L2, mRFP-GABARAP-L2; LIR(p62), LIR(p62)-mRFP-3xNLS or LIR(p62)-GFP); LIR(p62)m, LIR(p62)m-mRFP-3xNLS or LIR(p62)m-GFP.

Figure 2. Identification of selective mATG8-binding LIR motifs. (**a-b**) An LC3-interacting region (LIR) from SpHfl1 (LIR(Sp)) interacts preferentially with GABARAP-L2 proteins. **a**, Cellular localization of the LIR(Sp)-GFP and each mRFP-mATG8 in HKO cells (left) and quantification of the autophagosome and cytosol (A/C) ratio of GFP fluorescence. Values are presented as means + SEM ($n \geq 20$ for each group). ***P < 0.001 compared with all other groups. **b**, Glutathione S transferase (GST) pull-down assays to analyze the binding of LIR(Sp)-GFP. The coprecipitated LIR(Sp)-GFP protein was analyzed by western blot (WB) using the indicated anti-GFP antibodies. (**c-d**) A phosphomimetic LIR motif from Nix/BNIP-3L (LIR(Nix-p) interacts preferentially with GABARAP-L1. ***c,*** Quantification of the A/C ratio of GFP fluorescence in HKO cells coexpressing LIR(Nix-P)-GFP and each mRFP-mATG8. Values are presented as means + SEM ($n \geq 32$ for each group). ***P < 0.001 compared with all other groups. **d**, Glutathione S transferase (GST) pull-down assays to analyze the binding of LIR(Nix-p)-GFP. The coprecipitated LIR(Nix-p)-GFP protein was analyzed by western blot (WB) using the indicated anti-GFP antibodies. (E-F) An LIR motif from the ATG4B mutant LIR(4B(T)) interacts preferentially with GABARAP/GABARAP-L1 proteins. **e**, Quantification of the A/C ratio of GFP fluorescence in HKO cells expressing LIR(4B(T))-GFP and each mRFP-mATG8. Values are presented as means + SEM ($n \geq 20$ for each group). ***P < 0.001 compared with all other groups. **f**, Glutathione S transferase (GST) pull-down assays to analyze the binding of LIR(4B(T))-GFP. The coprecipitated LIR(4B(T))-GFP protein was analyzed by western blot (WB) using the indicated anti-GFP antibodies. (**g-h*)*** An LIR motif from the TP53INP2 mutant LIR(TP(T)) interacts preferentially with LC3C. ***g***, Quantification

of the A/C ratio of GFP fluorescence in HKO cells coexpressing LIR(TP(T))-GFP and each mRFP-mATG8 mATG8. Values are presented as means + SEM ($n \geq 20$ for each group). ***P < 0.001 compared with all other groups. **h**, Glutathione S transferase (GST) pull-down assays to analyze LIR(TP(T))-GFP binding. The coprecipitated LIR(TP(T))-GFP protein was analyzed by western blot (WB) using the indicated anti-GFP antibodies. LC3A, mRFP-LC3A; LC3B, mRFP-LC3B; LC3C, mRFP-LC3C; RAP, mRFP-GABARAP; RAP-L1, mRFP-GABARAP-L1; RAP-L2, mRFP-GABARAP-L2. For the GST pull-down assay, data from one representative experiment of three independent experiments is presented. Scale bar: 10 μm.

Figure 3. Structural basis for selective binding of mATG8-binding LIR motifs

(**a, c**) Crystal structure of SpHfl1 LIR-GABARAP-L2 complex (**a**) and LIR(TP)-GABARAP complex (**c**). Left, ribbon model. Right, electrostatic surface potentials of mATG8 proteins with a ribbon model of LIR peptides, where the side-chains of LIR residues involved in the interaction are shown as a stick model. **b**, Close-up view of the interactions between SpHfl1 LIR and GABARAP-L2. Possible electrostatic interactions are shown as a broken line. **d**, Modeled structure of the LIR(TP(T))-LC3C complex. Possible electrostatic or hydrogen-bond interactions are shown with a stick model. **e**, ITC data of mATG8 mutants with SpHfl1 LIR.

Figure 4. Selective mATG8-positive autophagosome targeting of gProbe-X. a, Schematic diagram of gProbe-X and its binding preference. X: Fy, TP(T), St, 4B(T), Sp, or Sp(I). **b**, Quantification of the GFP fluorescence intensities in the autophagosomes and cytosol (A/C ratio) of gProbe-X ($n \geq 20$ for each group). Values are presented as means + SEM. ***P < 0.001 compared with all other groups. (**c-g**) CLEM. **c**, CLEM images of mRFP-LC3A/B- and GFP-GABARAP-L2-coexpressing HeLa cells. The cells were treated with rapamycin (100 nM) in the presence of BafA1 (100 nM) for 2 h. Red indicates LC3, and green indicates GABARAP-

L2. Multiple transmission electron microscopy images were taken at 2500× magnification. The images were stitched to create a large field of view. The black dotted-line box shows the morphology of the autophagosome. N, nucleus; M, mitochondria; ER, endoplasmic reticulum. (D-G) Magnified autophagosome image by CLEM. (**d)**, Phagopore, (**e**) early autophagosome, and (**f, g**) late autophagosome are shown (left: CLEM, middle: electron microscopy image, right: fluorescence image). Scale bar: 10 μm.

Figure 5. Generation of selective mATG8-delipidating Deconjugase. a, Schematic diagram of Deconjugase-X and its binding preferences. **b**, Confocal images showing autophagosome formation of GFP-mATG8 protein coexpressed with Deconjugase-X in mouse embryonic fibroblasts (MEFs) upon autophagy induction (100 nM rapamycin, 4 h). Scale bar: 10 μm. X: Fy, TP(T), St, 4B(T), or Sp(I). Deconjugase$_{C258S}$, a catalytically inactive mutant, **c**, Bar graphs illustrate the autophagosome spot number for each cell. Values are presented as means + SEM (n ≥20 for each group). *P < 0.01 compared with Deconjugase$_{C258S}$-expressing cells. Rapa, rapamycin. (**d–f**) Representative western blots of four independent experiments of endogenous mATG8 proteins (**d**), p62 (**e**), or NDP52 (**f**) in HEK293T cells expressing Deconjugase-Fy or Deconjugase-Sp(I) upon autophagy induction (100 nM rapamycin [Rapa] for 4 h). 3xFLAG empty vector (FLAG) or Deconjugase was used as the control. A lysate of cells expressing 3xFLAG-LC3C was used in the LC3L detection experiment. Data from one representative experiment of three independent experiments is presented. LC3A, GFP-LC3A; LC3B, GFP-LC3B; LC3C, GFP-LC3C; RAP, GFP-GABARAP; RAP-L1, GFP-GABARAP-L1; RAP-L2, GFP-GABARAP-L2.

Figure 6. Regulation of TDP25-mediated aggregates by selective mATG8 deconjugases.

a, Confocal images showing TDP25-mediated aggregates in mouse cortical neurons expressing Deconjugase-X together with Myc-TDP-25. Scale bar: 10 μm. X: Fy, TP(T), St, 4B(T), or Sp(I). (**b-c**) Bar graphs show TDP-25 aggregate size (**b**) or number (**c**) per cell. Values are presented as means + SEM ($n \geq 17$ for each group). ***$P < 0.001$.

Table 1. Summary of the binding property of known LIR motifs to each lipidated mATG8.

Underline; core region in LIR motif. The A/C ratio: -1.4: - ; 1.4-2.0: +; 2.0-4.0: ++; 4.0: +++

LIR protein	LIR motif	LC3/GABARAP family interaction					
		LC3A	LC3B	LC3C	GABARAP	L1	L2
P62	SDNCSGGDDDWTHLSSKEVDPSTGE	+ (1.917±0.072, N=23)	+ (1.935±0.085, N=23)	+ (1.502±0.077, N=22)	- (1.072±0.037, N=23)	- (1.086±0.041, N=23)	- (1.051±0.028, N=23)
P62m	SDNCSGGDDDATHASSKEVDPSTGE	- (0.937±0.030, N=25)	- (0.996±0.026, N=25)	- (0.977±0.022, N=25)	- (1.004±0.025, N=25)	- (1.001±0.033, N=25)	- (0.9919±0.033, N=26)
SpHfl1 (Sp)	LQFEIDDEMEPLYNQAKQMRYGDY	- (1.050±0.035, N=20)	- (1.042±0.032, N=20)	- (1.047±0.040, N=20)	- (1.230±0.110, N=22)	+ (1.462±0.081, N=22)	++ (2.117±0.088, N=20)
SpHfl1(l) (Sp(l))	LQFEIDDEMEPIYNQAKQMRYGDY	- (1.051±0.032, N=15)	- (1.045±0.039, N=15)	- (0.923±0.047, N=16)	- (0.988±0.051, N=15)	- (0.874±0.039, N=16)	++ (2.754±0.211, N=15)
ALFY	DQLSLDEKDGFIFVNYSEGQTRAHL	- (1.335±0.041, N=15)	- (1.280±0.065, N=15)	+ (1.718±0.087, N=15)	++ (3.158±0.231, N=15)	++ (3.072±0.187, N=15)	++ (3.205±0.284, N=15)
AS67	SFTMYEPDQQTIVIES	- (1.145±0.044, N=20)	- (1.147±0.046, N=21)	++ (2.467±0.121, N=20)	- (1.017±0.044, N=20)	- (1.055±0.035, N=25)	- (1.018±0.048, N=20)
ATG4A	QLEEFDLEEDFEILSV	+ + (2.674±0.099, N=32)	++ (2.935±0.118, N=30)	- (1.282±0.041, N=34)	++ (2.121±0.130, N=27)	++ (2.187±0.118, N=30)	+ (1.455±0.072, N=30)
ATG4B (4B)	ERFFDSEDEDFEILSL	++ (2.687±0.116, N=32)	++ (2.694±0.107, N=31)	- (1.216±0.066, N=30)	++ (2.243±0.105, N=30)	++ (2.195±0.122, N=30)	++ (2.143±0.142, N=30)
ATG4B(T) (4B(T))	ERFFDSEDEDTEILSL	- (1.017±0.035, N=20)	- (1.039± 0.045, N=20)	- (1.101± 0.047, N=21)	++ (2.191± 0.234, N=20)	++ (2.305± 0.234, N=20)	- (0.979± 0.031, N=23)
ATG4C	KQLKRFSTEEFVLL	++ (2.160±0.078, N=34)	++ (2.130±0.087, N=32)	+ (1.449±0.053, N=30)	+ (1.838±0.091, N=22)	++ (2.934±0.122, N=29)	+ (1.921±0.094, N=28)
ATG4D	LRAKRPSSEDFVFL	++ (2.204±0.122, N=30)	++ (2.209±0.104, N=30)	+ (1.597±0.067, N=30)	+ (1.825±0.069, N=30)	++ (2.653±0.112, N=30)	+ (1.952±0.088, N=30)
ATG13	GGSSGNTHDDFVMIDFKPAFSKDDI	- (1.274±0.070, N=16)	- (1.219±0.091, N=18)	- (1.169±0.067, N=15)	- (1.142±0.048, N=18)	- (1.083±0.051, N=17)	- (1.100±0.052, N=15)
BNIP3	GMQEESLQGSWVELHFSNNGNGGSV	+ (1.597±0.119, N=15)	+ (1.670±0.113, N=15)	+ (1.547±0.129, N=17)	+ (1.575±0.112, N=15)	+ (1.456±0.062, N=15)	+ (1.575±0.082, N=15)
FAIM2	APTAVPLHPSWAYVDPSSSSSYDNG	+ (1.937±0.101, N=21)	+ (1.986±0.099, N=22)	+ (1.798±0.103, N=20)	- (1.338±0.048, N=22)	- (1.260±0.050, N=21)	- (1.350±0.041, N=20)
FAM134B	EDTDTEEGDDFELLDQSELDQIESE	++ (2.080±0.099, N=15)	+ (1.806±0.088, N=15)	- (0.951±0.052, N=16)	+ (1.828±0.158, N=15)	++ (2.152±0.135, N=15)	- (1.037±0.035, N=18)
FIP200	PDSIDAHTFDFETIPHPNIEQTIHQ	- (1.199±0.041, N=20)	- (1.176±0.076, N=21)	- (1.176±0.054, N=21)	- (1.146±0.055, N=21)	- (1.138±0.032, N=20)	- (1.140±0.043, N=24)
FUNDC1	PQDYESDDDSYEVLDLTEYARRHQW	+ (1.871±0.108, N=16)	++ (2.067±0.103, N=15)	++ (2.188±0.142, N=15)	+ (1.860±0.130, N=17)	+ (1.965±0.154, N=17)	+ (1.879±0.130, N=15)
Fyco1 (Fy)	TDYRPPDDAVFDIITDEELCQIQES	++ (3.824±0.150, N=20)	+++ (4.035±0.138, N=20)	+ (1.837±0.096, N=20)	- (1.196±0.054, N=20)	- (1.127±0.060, N=20)	- (1.171±0.033, N=20)
JMY	FALEETLESDWVAVRPHVFDEREKH	- (1.264±0.083, N=15)	- (1.211±0.085, N=16)	- (1.271±0.078, N=16)	+ (1.430±0.078, N=17)	+ (1.463±0.141, N=15)	+ (1.455±0.117, N=15)
NBR1	QSQSSASSEDYIIILPECFDTSRPL	- (1.111±0.034, N=16)	- (1.093±0.042, N=15)	- (1.108±0.037, N=18)	- (0.985±0.042 N=15)	- (1.029±0.049, N=15)	- (1.046±0.046, N=15)
Nix/BNIP-3L	LPPPAGLNSSWVELPMNSSNGNDNG	- (0.914±0.027, N=15)	- (1.041±0.041, N=15)	- (0.974±0.035, N=16)	- (0.990±0.044, N=15)	- (1.070±0.033, N=15)	- (1.030±0.038, N=15)
Nix-p	LPPPAGLNEEWVELPMNSSNGNDNG	- (1.048±0.030, N=32)	- (1.042±0.031, N=30)	- (1.022±0.024, N=31)	- (1.043±0.030, N=32)	+ (1.989±0.104, N=30)	- (1.046±0.040, N=30)
PLEKHM	QKVRPQQEDEWVNVQYPDQPEEPPE	+ (1.440±0.095, N=15)	- (1.284±0.066, N=15)	+ (1.533±0.110, N=15)	++ (2.064±0.129, N=15)	+ (1.866±0.095, N=15)	+ (1.948±0.130, N=15)
Stbd1 (St)	NSQDRVDHEEWEMVPRHSSWGDVGV	- (1.018±0.038, N=20)	- (0.983±0.030, N=20)	- (1.055±0.047, N=20)	++ (3.704±0.105, N=20)	+++ (5.099±0.173, N=20)	+++ (4.831±0.204, N=20)
Tax1Bp1	TMEDEGNSDMLVVTTKAGLLELKIE	- (1.213±0.026, N=15)	- (1.208±0.039, N=18)	- (1.290±0.055, N=15)	- (1.250±0.066, N=15)	- (1.142±0.070, N=16)	- (1.290±0.065, N=15)
TBC1D25	PSEDSPLLEDWDIISPKDVIGSDVL	++ (2.320±0.130, N=21)	++ (2.278±0.121, N=22)	+ (1.564±0.054, N=25)	- (1.295±0.049, N=23)	+ (1.415±0.107, N=23)	- (1.351±0.049, N=22)
TECPR2	DLEDEWEVI	- (1.354±0.083, N=19)	+ (1.507±0.099, N=17)	+ (1.701±0.106, N=19)	+ (1.583±0.144, N=17)	+ (1.755±0.123, N=18)	+ (1.460±0.108, N=16)
TP53INP1	PEFNEKEDDEWILVDFIDTCTGFSA	++ (2.009±0.097, N=15)	+ (1.801±0.090, N=15)	++ (2.748±0.129, N=15)	++ (2.199±0.164, N=15)	++ (2.447±0.192, N=15)	++ (3.321±0.237, N=15)
TP53INP2 (TP)	FVSEEDEVDGWLIIDLPDSYAAPPS	++ (2.519±0.050, N=27)	++ (2.452±0.095, N=20)	+++ (4.581±0.154, N=20)	+++ (5.277±0.137, N=20)	+++ (5.016±0.141, N=20)	+++ (4.320±0.174, N=20)
TP53INP2(T) (TP(T))	FVSEEDEVDGTLIIDLPDSYAAPPS	- (1.078±0.041, N=20)	- (1.072±0.030, N=20)	++ (2.453±0.078, N=20)	- (1.021±0.036, N=22)	- (1.003±0.030, N=20)	- (1.030±0.039, N=21)
UBR4	QEQSEVDHGDFEMVSESMVLETAEN	+ (1.477±0.096, N=15)	+ (1.526±0.103, N=15)	+ (1.683±0.189, N=15)	++ (2.204±0.135, N=15)	++ (2.826±0.160, N=15)	+ (1.611±0.106, N=16)
ULK1	SKDSSCDTDDFVMVPAQFPGDLVAE	- (1.049±0.032, N=28)	- (1.140±0.027, N=28)	- (1.231±0.035, N=23)	+ (1.609±0.074, N=23)	+ (1.588±0.073, N=24)	+ (1.627±0.091, N=26)
ULK2	SKNSSCDTDDFVLVPHNISSDHSCD	- (1.015±0.037, N=15)	- (0.950±0.041, N=15)	- (1.391±0.071, N=15)	++ (2.328±0.177, N=15)	++ (2.503±0.158, N=15)	+ (1.965±0.158, N=17)

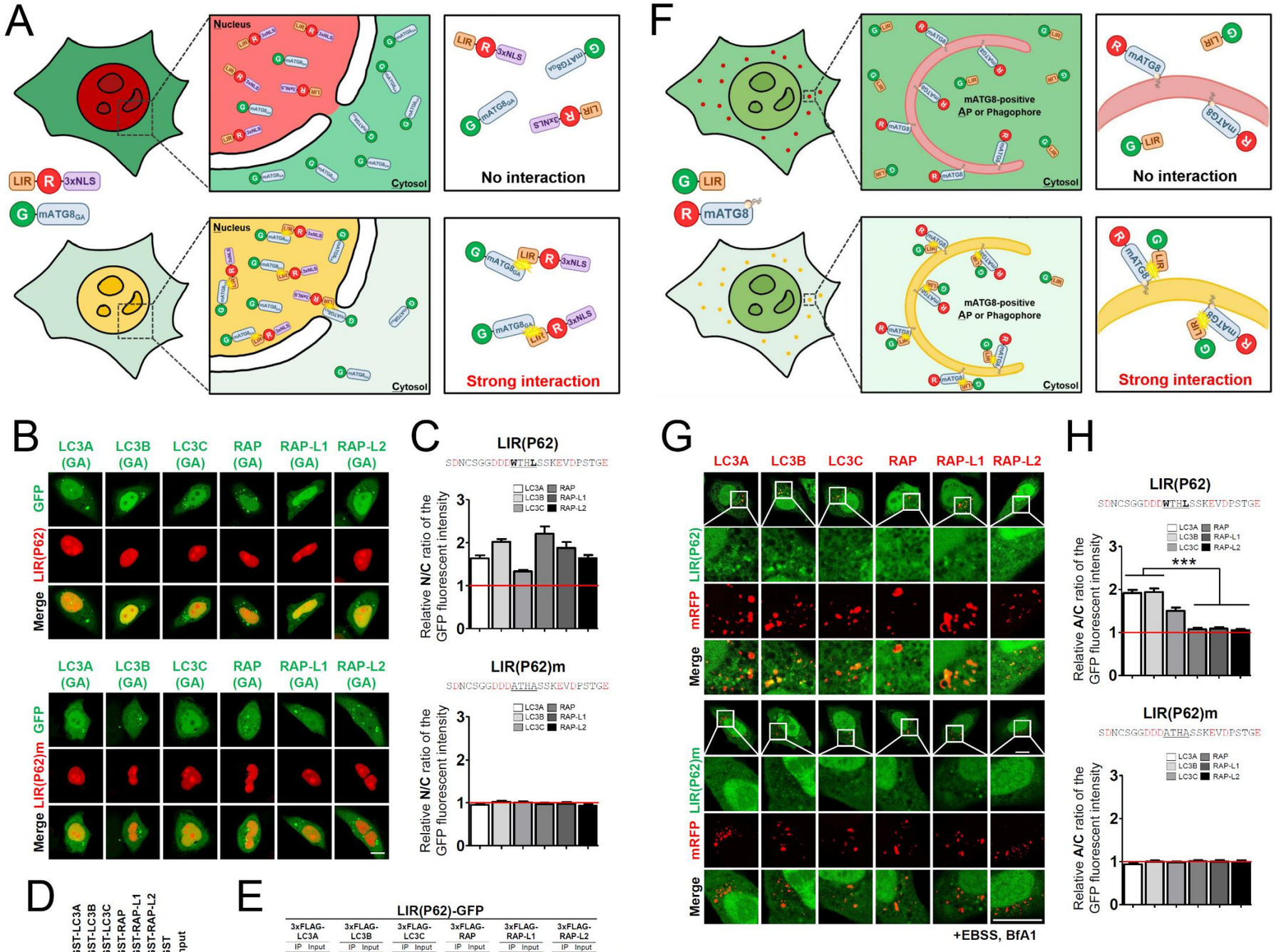
A
Nucleus
Cytosol
LIR
3xNLS
mATG8GA
No interaction
Strong interaction
F
mATG8-positive
AP or Phagophore
mATG8
B
LC3A (GA)
LC3B (GA)
LC3C (GA)
RAP (GA)
RAP-L1 (GA)
RAP-L2 (GA)
GFP
LIR(P62)
Merge
LIR(P62)m
C
LIR(P62)
SDNCSGGDDDWTHLSSKEVDPSTGE
LIR(P62)m
SDNCSGGDDDATHASSKEVDPSTGE
Relative N/C ratio of the GFP fluorescent intensity
LC3A
LC3B
LC3C
RAP
RAP-L1
RAP-L2
G
mRFP
+EBSS, BfA1
H
***
Relative A/C ratio of the GFP fluorescent intensity
D
GST-LC3A
GST-LC3B
GST-LC3C
GST-RAP
GST-RAP-L1
GST-RAP-L2
GST
Input
Anti-GFP
Coomassie
LIR(P62)-GFP
LIR(P62)m-GFP
E
LIR(P62)-GFP
LIR(P62)m-GFP
3xFLAG-LC3A
3xFLAG-LC3B
3xFLAG-LC3C
3xFLAG-RAP
3xFLAG-RAP-L1
3xFLAG-RAP-L2
IP
Input
Anti-GFP
Anti-FLAG

Figure 1

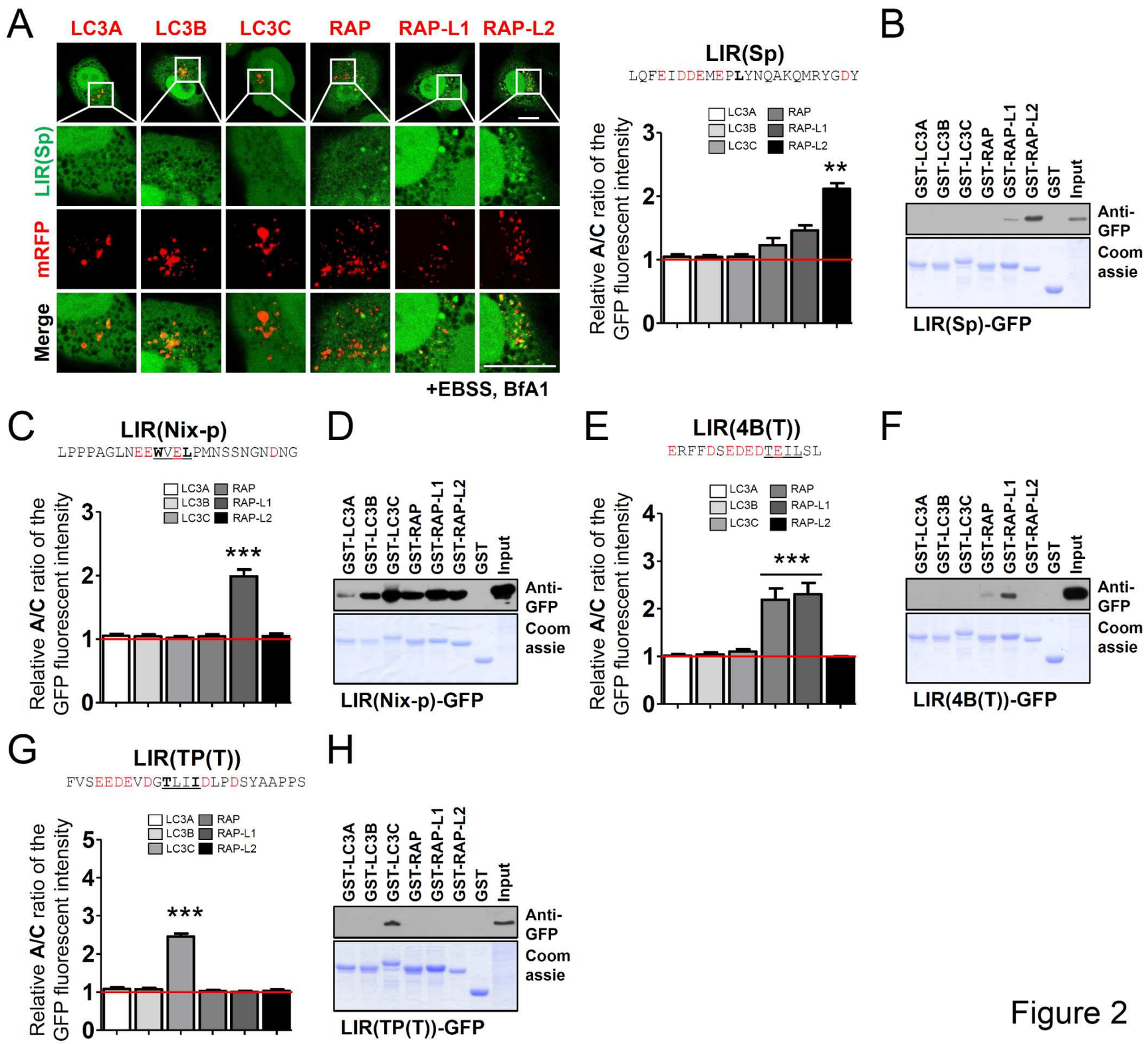
A
LC3A
LC3B
LC3C
RAP
RAP-L1
RAP-L2
LIR(Sp)
mRFP
Merge
+EBSS, BfA1
LIR(Sp)
LQFEIDDEMEPLYNQAKQMRYGDY
Relative A/C ratio of the GFP fluorescent intensity
**
B
GST-LC3A
GST-LC3B
GST-LC3C
GST-RAP
GST-RAP-L1
GST-RAP-L2
GST
Input
Anti-GFP
Coomassie
LIR(Sp)-GFP
C
LIR(Nix-p)
LPPPAGLNEEWVELPMNSSNGNDNG
***
LIR(Nix-p)-GFP
D
E
LIR(4B(T))
ERFFDSEDEDTEILSL
LIR(4B(T))-GFP
F
G
LIR(TP(T))
FVSEEDEVDGTLIIDLPDSYAAPPS
LIR(TP(T))-GFP
H

Figure 2

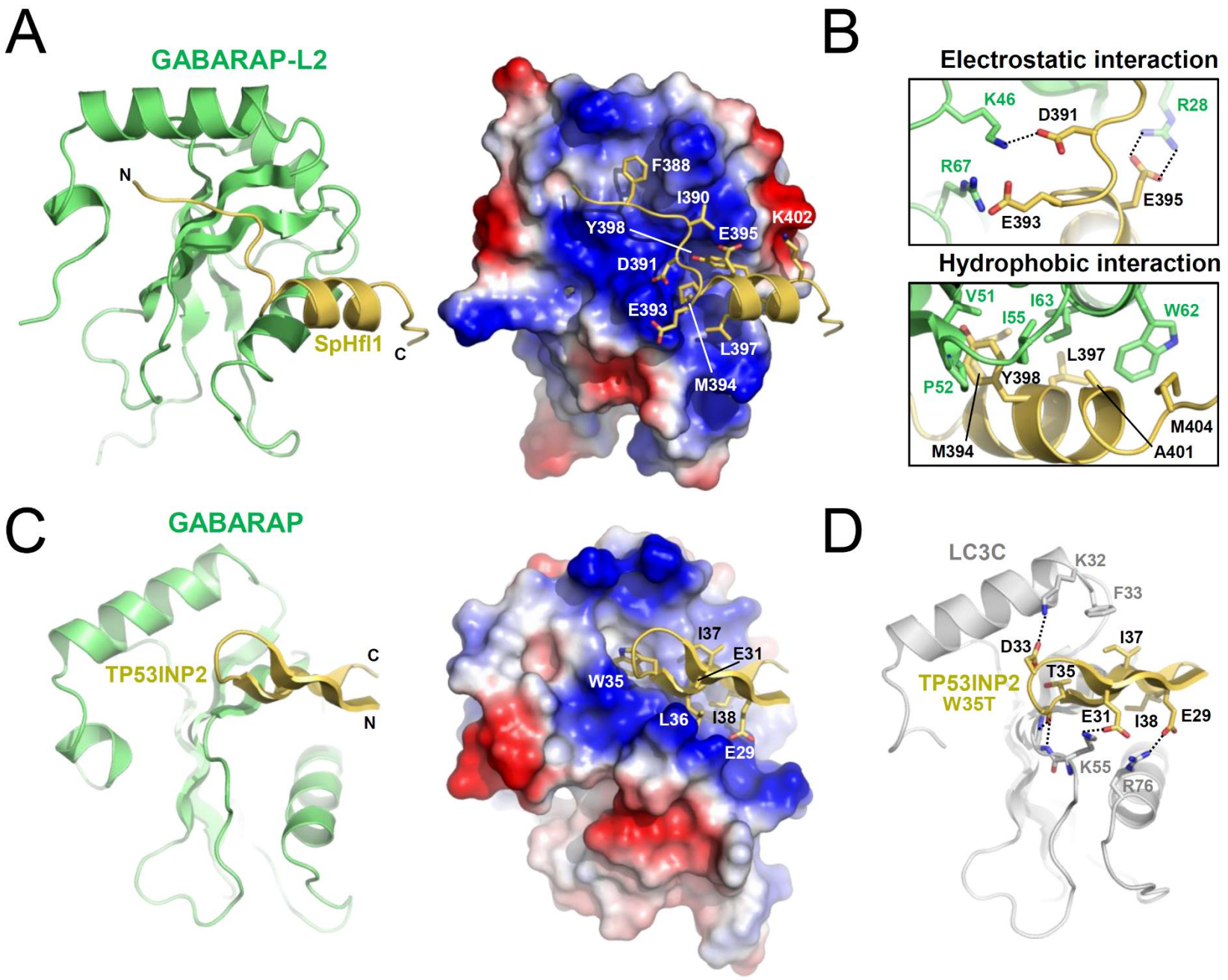
A
GABARAP-L2
N
SpHfl1
C
F388
I390
Y398
E395
K402
D391
E393
L397
M394
B
Electrostatic interaction
K46
D391
R28
R67
E395
E393
Hydrophobic interaction
V51
I63
W62
I55
L397
P52
Y398
M404
M394
A401
C
GABARAP
TP53INP2
C
N
I37
E31
W35
L36
I38
E29
D
LC3C
K32
F33
I37
D33
T35
TP53INP2
W35T
E31
I38
E29
K55
R76

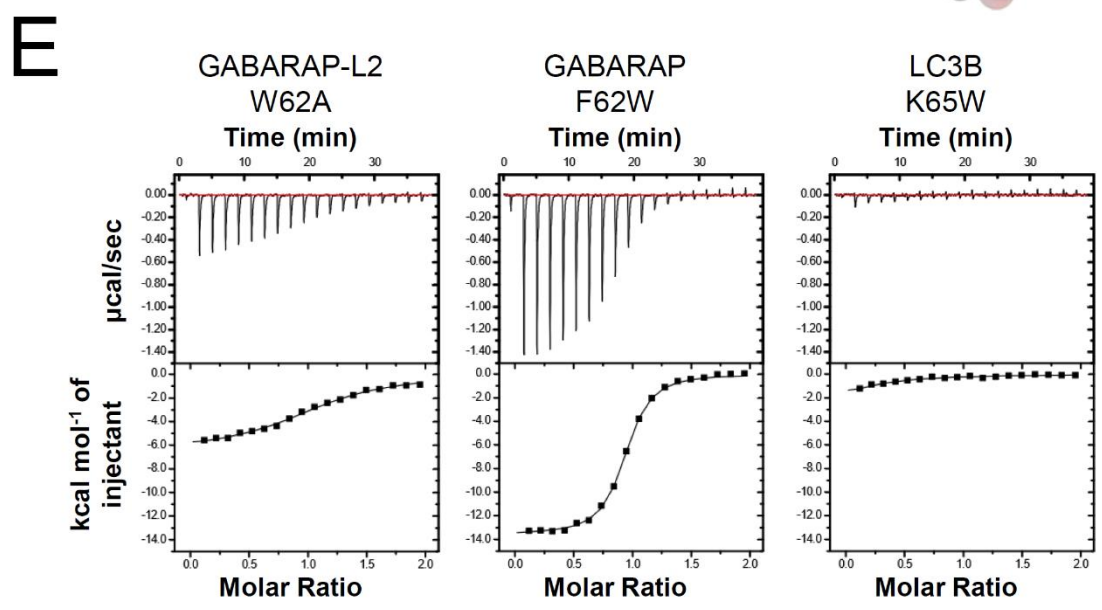
E
GABARAP-L2
W62A
GABARAP
F62W
LC3B
K65W
Time (min)
µcal/sec
kcal mol-1 of injectant
Molar Ratio
Kd (µM) 6.944 ± 0.699
0.629 ± 0.038
22.422 ± 8.446

Figure 3

A

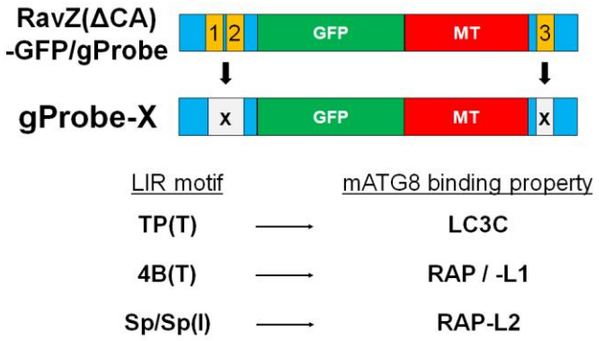
RavZ(ΔCA)
-GFP/gProbe
1
2
GFP
MT
3
gProbe-X
x
GFP
MT
x
LIR motif
mATG8 binding property
TP(T)
LC3C
4B(T)
RAP / -L1
Sp/Sp(I)
RAP-L2

B

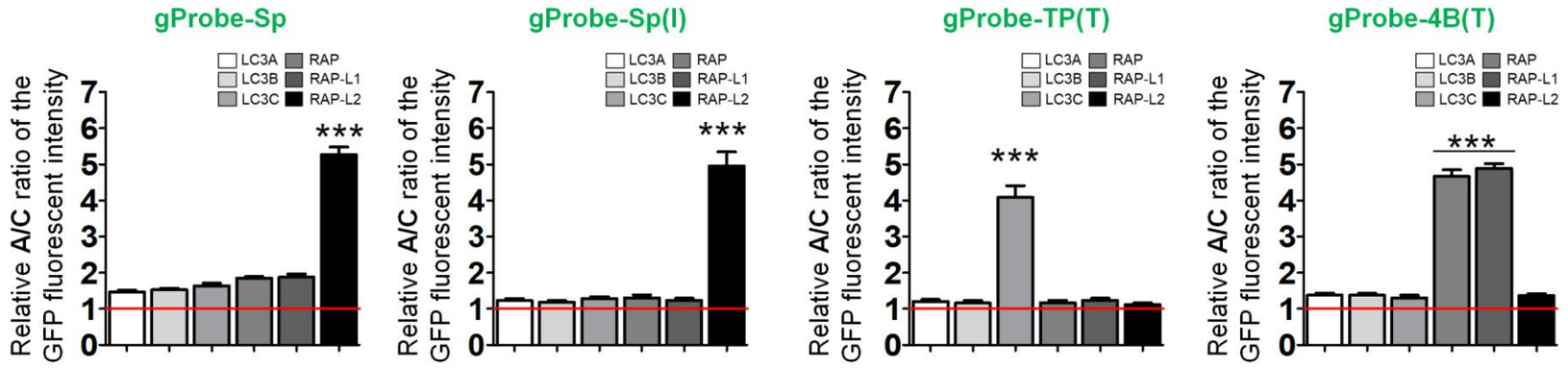
gProbe-Sp
gProbe-Sp(I)
gProbe-TP(T)
gProbe-4B(T)
LC3A
LC3B
LC3C
RAP
RAP-L1
RAP-L2
Relative A/C ratio of the GFP fluorescent intensity
***
0
1
2
3
4
5
6
7

C

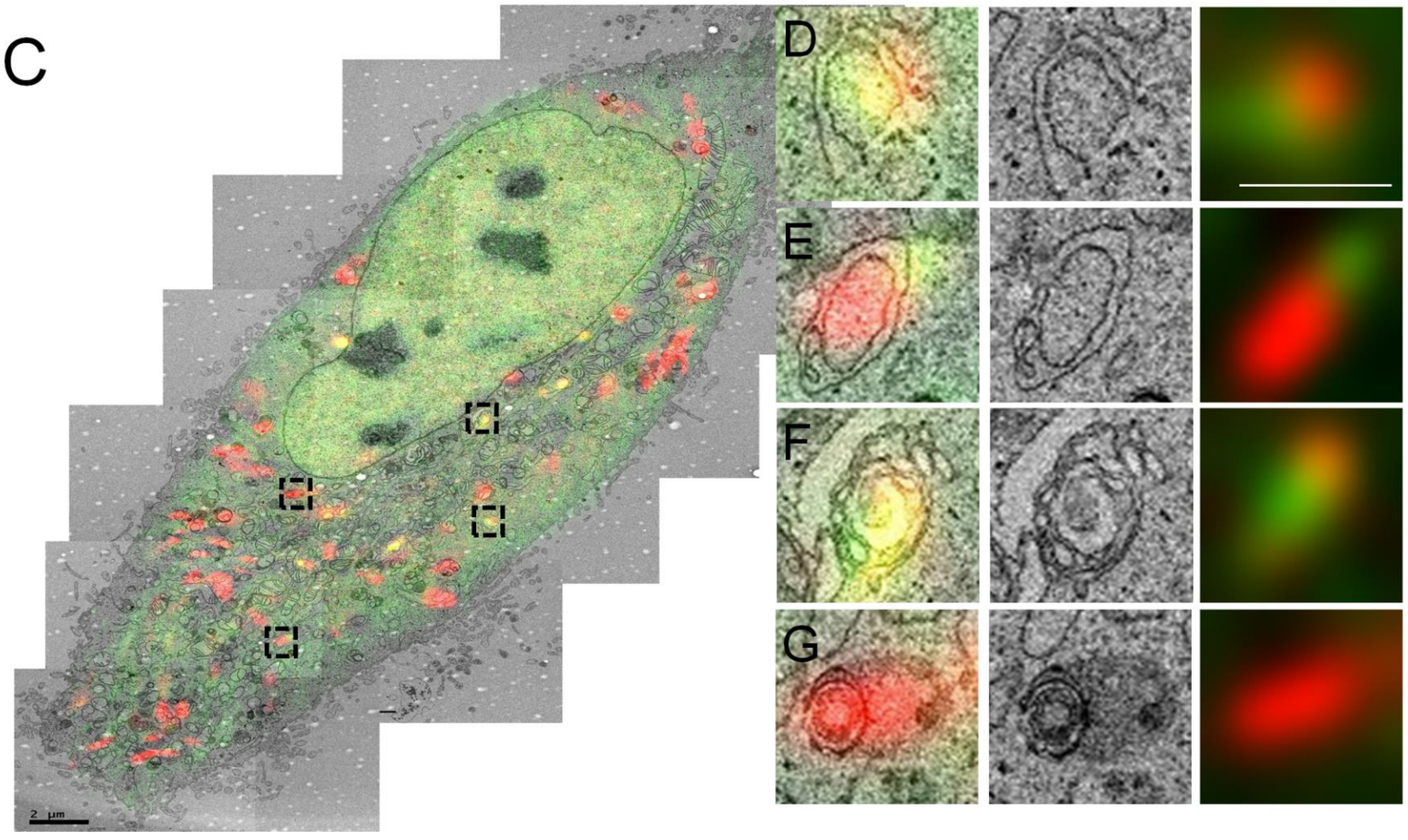
2 μm
D
E
F
G

Figure 4

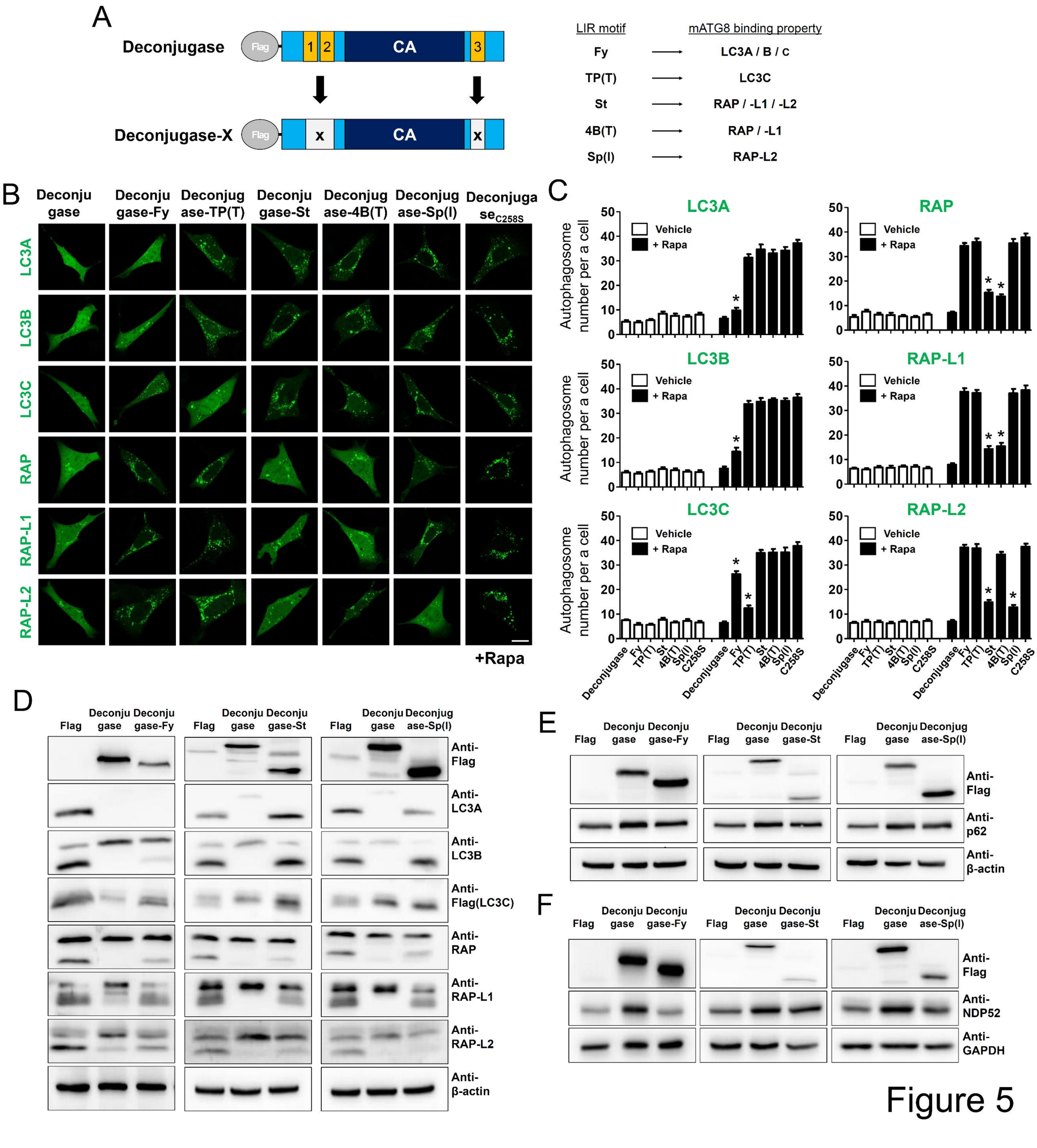
A
Deconjugase
Flag
1
2
CA
3
Deconjugase-X
Flag
x
CA
x
LIR motif
mATG8 binding property
Fy → LC3A / B / C
TP(T) → LC3C
St → RAP / -L1 / -L2
4B(T) → RAP / -L1
Sp(I) → RAP-L2
B
Deconjugase
Deconjugase-Fy
Deconjugase-TP(T)
Deconjugase-St
Deconjugase-4B(T)
Deconjugase-Sp(I)
Deconjugase C258S
LC3A
LC3B
LC3C
RAP
RAP-L1
RAP-L2
+Rapa
C
LC3A
RAP
LC3B
RAP-L1
LC3C
RAP-L2
Autophagosome number per a cell
Vehicle
+ Rapa
Deconjugase
Fy
TP(T)
St
4B(T)
Sp(I)
C258S
D
Flag
Deconjugase
Deconjugase-Fy
Deconjugase-St
Deconjugase-Sp(I)
Anti-Flag
Anti-LC3A
Anti-LC3B
Anti-Flag(LC3C)
Anti-RAP
Anti-RAP-L1
Anti-RAP-L2
Anti-β-actin
E
Anti-Flag
Anti-p62
Anti-β-actin
F
Anti-Flag
Anti-NDP52
Anti-GAPDH

Figure 5

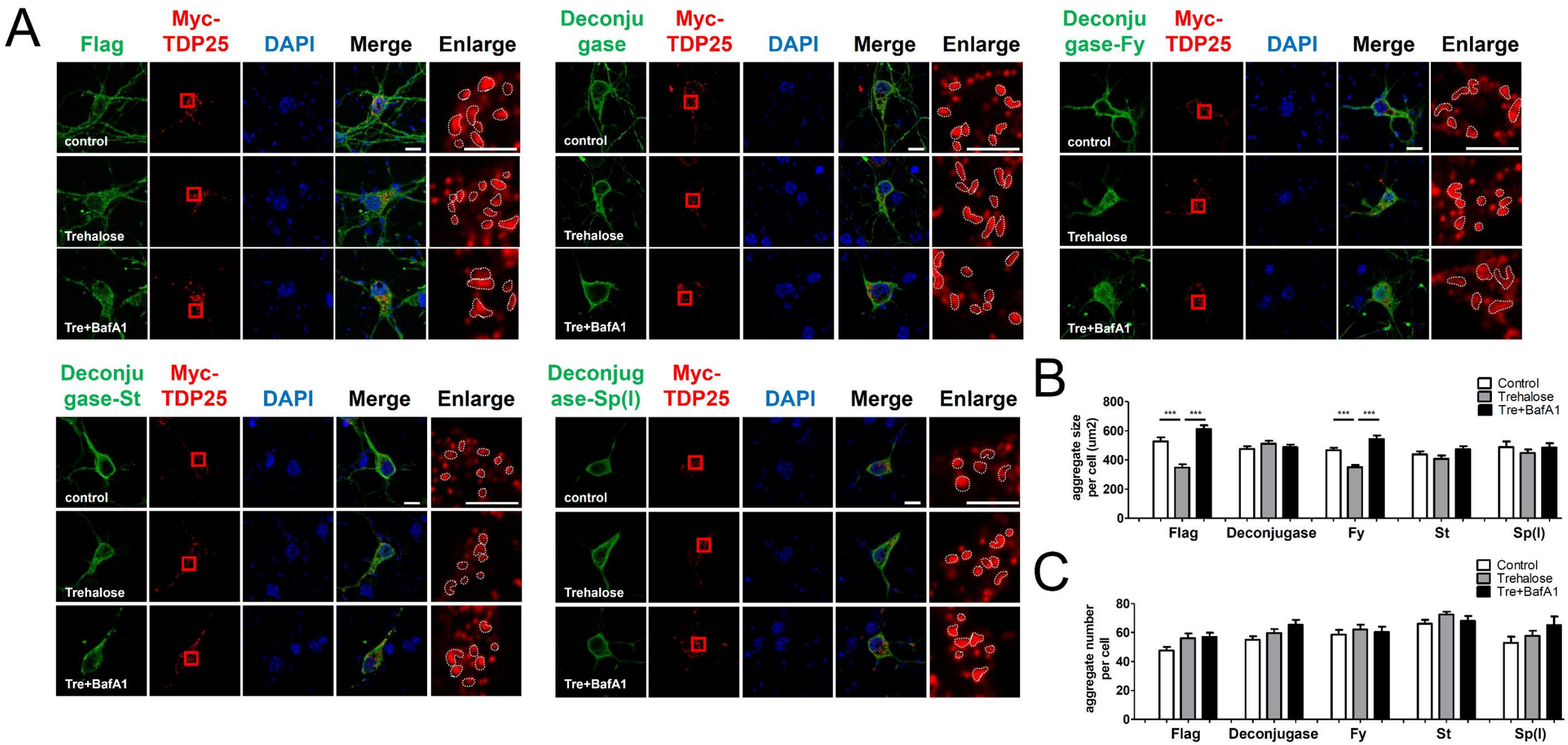
A
Flag
Myc-TDP25
DAPI
Merge
Enlarge
Deconjugase
Deconjugase-Fy
Deconjugase-St
Deconjugase-Sp(I)
control
Trehalose
Tre+BafA1
B
Control
Trehalose
Tre+BafA1
aggregate size per cell (um2)
Flag
Deconjugase
Fy
St
Sp(I)
C
aggregate number per cell

Figure 6

Figures

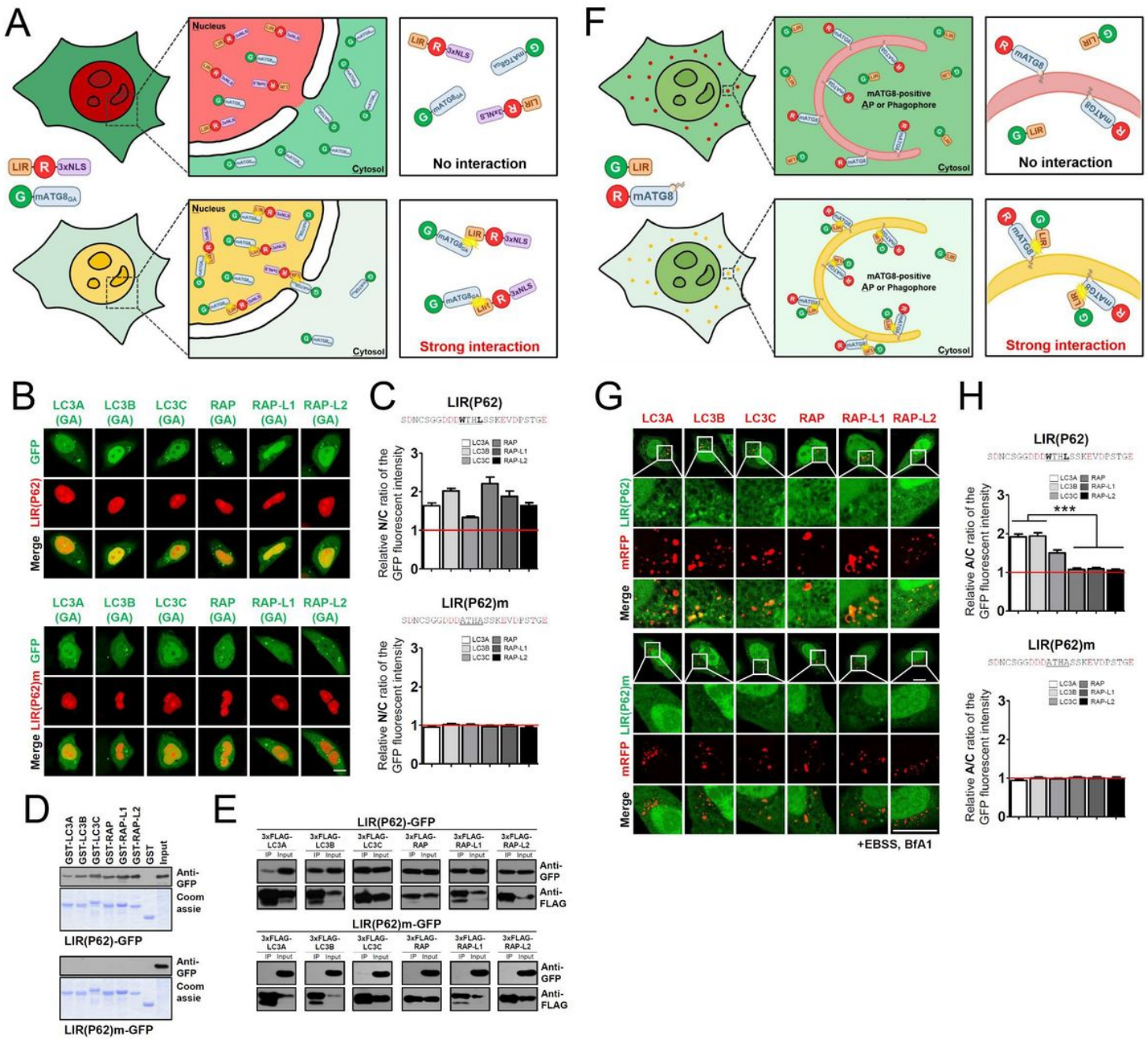

Figure 1

Development of new methods to detect the binding affinities of LIR motifs for non-lipidated or lipidated mATG8 proteins in vivo. a, Schematic model of the detection of binding affinities of LIR motifs toward non-lipidated mATG8 proteins in HKO cells using LIR(x)-mRFP-3xNLS and GFP-mATG8(GA) constructs. LIR: LC3-interacting region motif, NLS: nuclear localization signal or sequence, mATG8: mammalian ATG8. (b-c) The LIR motif from p62 (LIR(p62)) interacts with all non-lipidated mATG8 proteins. b, Cellular localization of LIR(p62)-mRFP-3xNLS or LIR(p62)m-mRFP-3xNLS LIR motif mutants, in which some amino acids in the consensus sequence of LIR(p62) were mutated to alanine in HKO cells. c,

Quantification of the nuclear and cytosolic (N/C) ratio of GFP fluorescence. Values are presented as means + SEM (n ≥ 20 for each group). (d-e) Glutathione S transferase (GST) pull-down assays (d) and 3xFLAG co-immunoprecipitation (co-IP) experiments (e) to analyze the binding of LIR(p62)-GFP and LIR(p62)m-GFP. The coprecipitated LIR(62)-GFP proteins (upper panel) were analyzed by western blot (WB) using the indicated anti-GFP antibodies. The immobilized GST fusion proteins used are displayed on Coomassie brilliant blue-stained gels (lower panel). Data from one representative experiment of three independent experiments is presented. f, Schematic model of the detection of binding affinities of LIR motifs toward lipidated mATG8 proteins in HKO cells using LIR(x)-GFP and mRFP-mATG8 constructs. (g-h) The LIR motif from p62 (LIR(p62)) interacts with lipidated LC3 subfamily proteins. g, Cellular localization of LIR(p62)- or LIR(p62)m-GFP and each mRFP-mATG8 in HKO cells. Scale bar: 10 μm. h, Quantification of the autophagosome and cytosol (A/C) ratio of GFP fluorescence. Values are presented as means + SEM (n ≥20 for each group). ***P < 0.001. Scale bar: 10 μm. LC3A(GA), GFP-LC3A(GA); LC3B(GA), GFP-LC3B(GA); LC3C(GA), GFP-LC3C(GA); RAP(GA), GFP-GABARAP(GA); RAP-L1(GA), GFP-GABARAP-L1(GA); RAP-L2(GA), GFP-GABARAP-L2(GA); LC3A, mRFP-LC3A; LC3B, mRFP-LC3B;37 LC3C, mRFP-LC3C; RAP, mRFP-GABARAP; RAP-L1, mRFP-GABARAP-L1; RAP-L2, mRFP-GABARAP-L2; LIR(p62), LIR(p62)-mRFP-3xNLS or LIR(p62)-GFP); LIR(p62)m, LIR(p62)m-mRFP-3xNLS or LIR(p62)m-GFP.

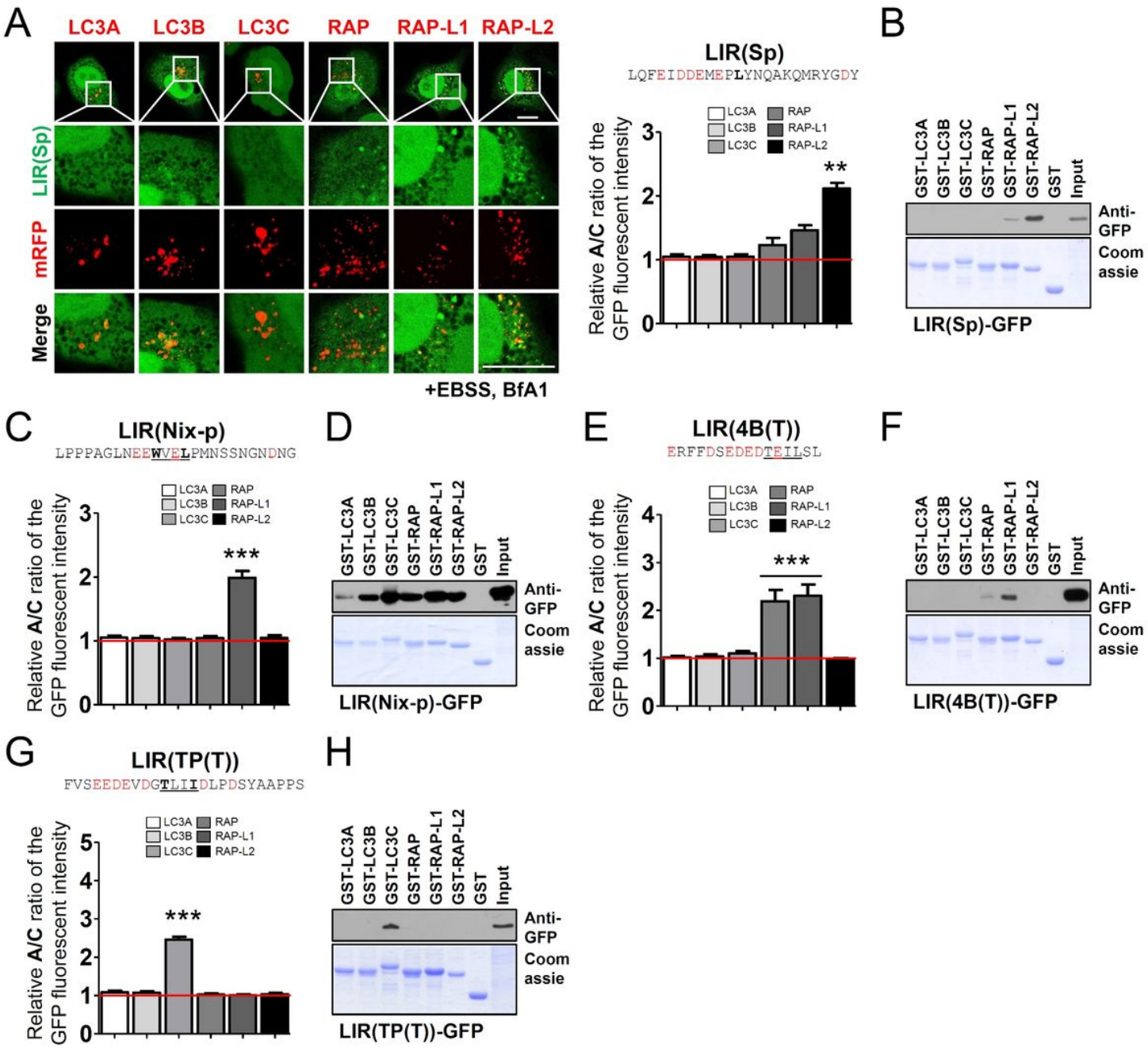

Figure 2

dentification of selective mATG8-binding LIR motifs. (a-b) An LC3-interacting region (LIR) from SpHfl1 (LIR(Sp)) interacts preferentially with GABARAP-L2 proteins. a, Cellular localization of the LIR(Sp)-GFP and each mRFP-mATG8 in HKO cells (left) and quantification of the autophagosome and cytosol (A/C) ratio of GFP fluorescence. Values are presented as means + SEM (n ≥20 for each group). ***P < 0.001 compared with all other groups. b, Glutathione S transferase (GST) pull-down assays to analyze the binding of LIR(Sp)-GFP. The coprecipitated LIR(Sp)-GFP protein was analyzed by western blot (WB) using the indicated anti-GFP antibodies. (c-d) A phosphomimetic LIR motif from Nix/BNIP-3L (LIR(Nix-p) interacts preferentially with GABARAP-L1. c, Quantification of the A/C ratio of GFP fluorescence in HKO cells coexpressing LIR(Nix-P)-GFP and each mRFP-mATG8. Values are presented as means + SEM (n ≥32

for each group). ***P < 0.001 compared with all other groups. d, Glutathione S transferase (GST) pull-down assays to analyze the binding of LIR(Nix-p)-GFP. The coprecipitated LIR(Nix-p)-GFP protein was analyzed by western blot (WB) using the indicated anti-GFP antibodies. (E-F) An LIR motif from the ATG4B mutant LIR(4B(T)) interacts preferentially with GABARAP/GABARAP-L1 proteins. e, Quantification of the A/C ratio of GFP fluorescence in HKO cells expressing LIR(4B(T))-GFP and each mRFP-mATG8. Values are presented as means + SEM (n ≥20 for each group). ***P < 0.001 compared with all other groups. f, Glutathione S transferase (GST) pull-down assays to analyze the binding of LIR(4B(T))-GFP. The coprecipitated LIR(4B(T))-GFP protein was analyzed by western blot (WB) using the indicated anti-GFP antibodies. (g-h) An LIR motif from the TP53INP2 mutant LIR(TP(T)) interacts preferentially with LC3C. g, Quantification of the A/C ratio of GFP fluorescence in HKO cells coexpressing LIR(TP(T))-GFP and each mRFP-mATG8 mATG8. Values are presented as means + SEM (n ≥20 for each group). ***P < 0.001 compared with all other groups. h, Glutathione S transferase (GST) pull-down assays to analyze LIR(TP(T))-GFP binding. The coprecipitated LIR(TP(T))-GFP protein was analyzed by western blot (WB) using the indicated anti-GFP antibodies. LC3A, mRFP-LC3A; LC3B, mRFP-LC3B; LC3C, mRFP-LC3C; RAP, mRFP-GABARAP; RAP-L1, mRFP-GABARAP-L1; RAP-L2, mRFP-GABARAP-L2. For the GST pull-down assay, data from one representative experiment of three independent experiments is presented. Scale bar: 10 μm.

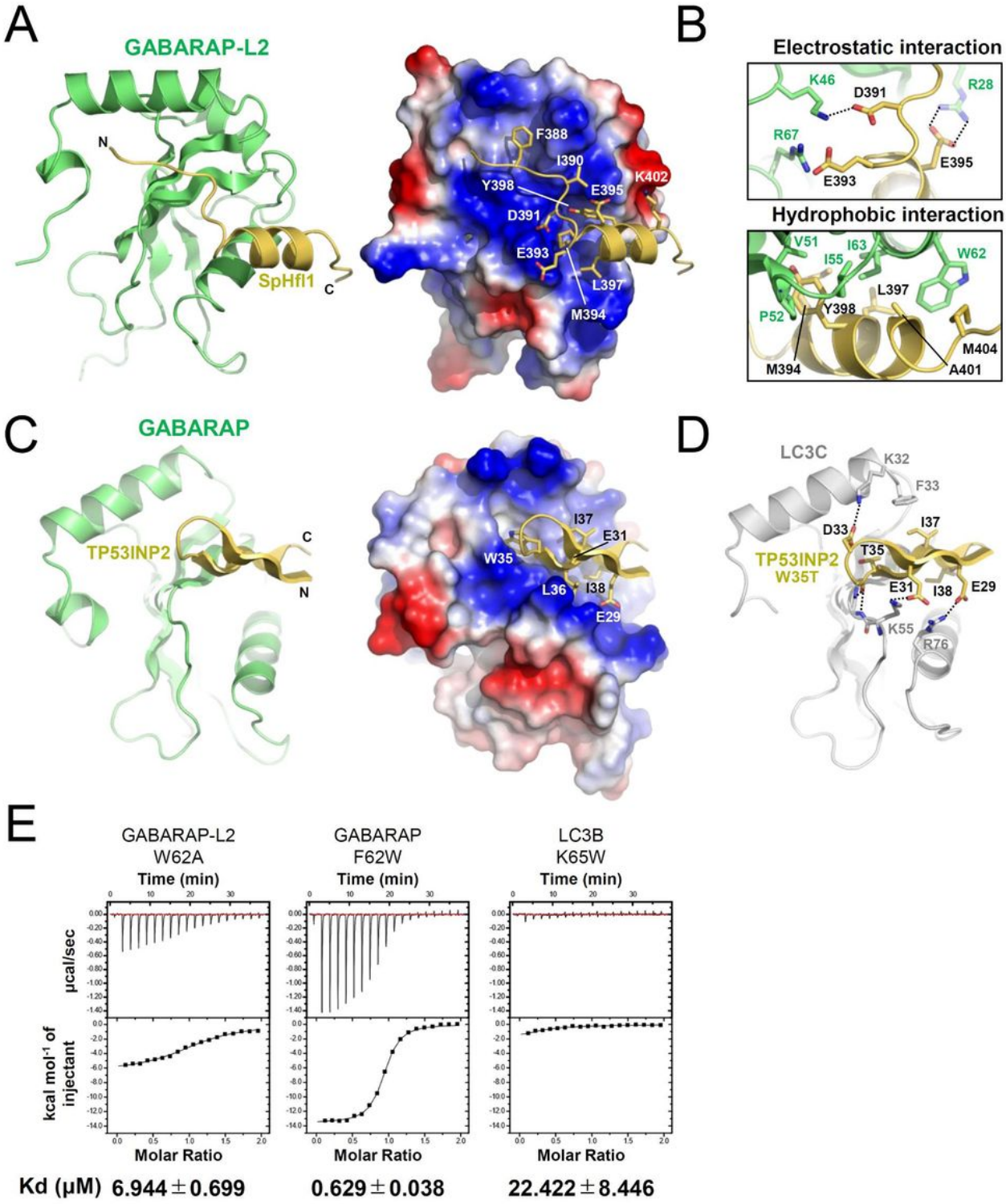

Figure 3

Structural basis for selective binding of mATG8-binding LIR motifs (a, c) Crystal structure of SpHfl1 LIR-GABARAP-L2 complex (a) and LIR(TP)-GABARAP complex (c). Left, ribbon model. Right, electrostatic surface potentials of mATG8 proteins with a ribbon model of LIR peptides, where the side-chains of LIR residues involved in the interaction are shown as a stick model. b, Close-up view of the interactions between SpHfl1 LIR and GABARAP-L2. Possible electrostatic interactions are shown as a broken line. d,

Modeled structure of the LIR(TP(T))-LC3C complex. Possible electrostatic or hydrogen-bond interactions are shown with a stick model. e, ITC data of mATG8 mutants with SpHfl1 LIR.

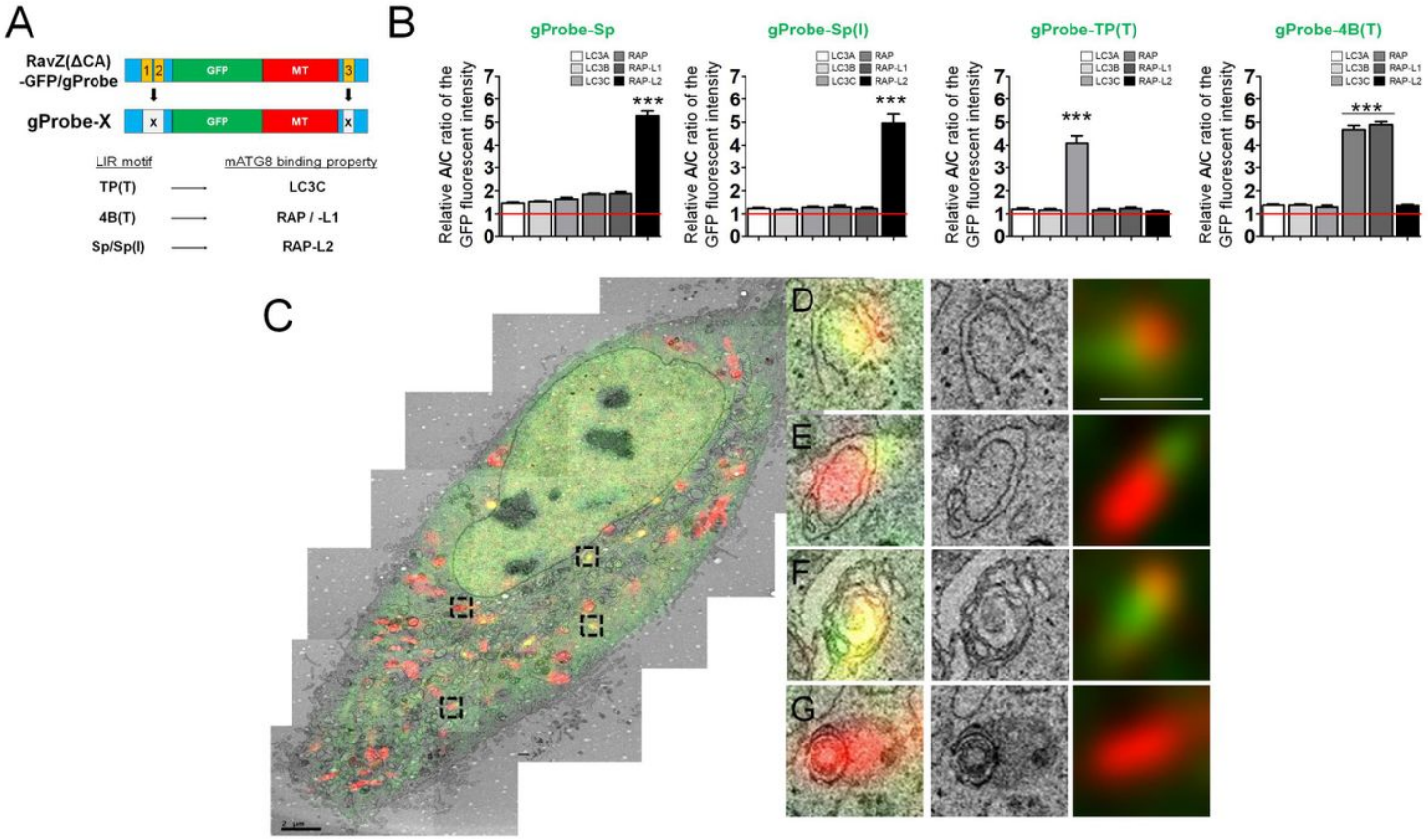

Figure 4

Selective mATG8-positive autophagosome targeting of gProbe-X. a, Schematic diagram of gProbe-X and its binding preference. X: Fy, TP(T), St, 4B(T), Sp, or Sp(I). b, Quantification of the GFP fluorescence intensities in the autophagosomes and cytosol (A/C ratio) of gProbe-X (n ≥20 for each group). Values are presented as means + SEM. ***P < 0.001 compared with all other groups. (c-g) CLEM. c, CLEM images of mRFP-LC3A/B- and GFP-GABARAP-L2-coexpressing HeLa cells. The cells were treated with rapamycin (100 nM) in the presence of BafA1 (100 nM) for 2 h. Red indicates LC3, and green indicates GABARAP-L2. Multiple transmission electron microscopy images were taken at 2500× magnification. The images were stitched to create a large field of view. The black dotted-line box shows the morphology of the autophagosome. N, nucleus; M, mitochondria; ER, endoplasmic reticulum. (D-G) Magnified autophagosome image by CLEM. (d), Phagopore, (e) early autophagosome, and (f, g) late autophagosome are shown (left: CLEM, middle: electron microscopy image, right: fluorescence image). Scale bar: 10 μm.

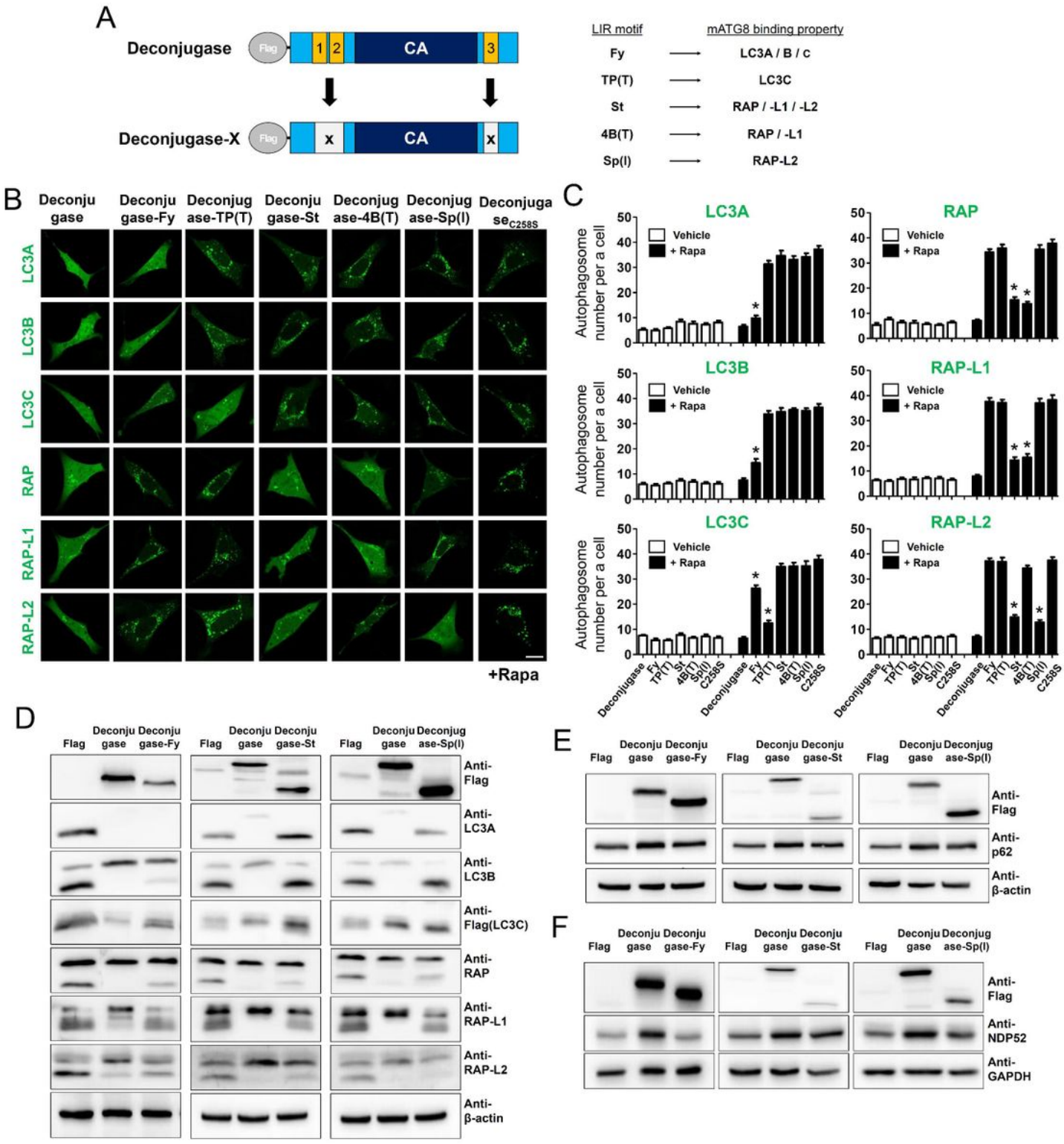

Figure 5

Generation of selective mATG8-delipidating Deconjugase. a, Schematic diagram of Deconjugase-X and its binding preferences. b, Confocal images showing autophagosome formation of GFP-mATG8 protein coexpressed with Deconjugase-X in mouse embryonic fibroblasts (MEFs) upon autophagy induction (100 nM rapamycin, 4 h). Scale bar: 10 μm. X: Fy, TP(T), St, 4B(T), or Sp(I). DeconjugaseC258S, a catalytically inactive mutant, c, Bar graphs illustrate the autophagosome spot number for each cell. Values are

presented as means + SEM (n ≥20 for each group). *P < 0.01 compared with DeconjugaseC258S-expressing cells. Rapa, rapamycin. (d–f) Representative western blots of four independent experiments of endogenous mATG8 proteins (d), p62 (e), or NDP52 (f) in HEK293T cells expressing Deconjugase-Fy or Deconjugase-Sp(I) upon autophagy induction (100 nM rapamycin [Rapa] for 4 h). 3xFLAG empty vector (FLAG) or Deconjugase was used as the control. A lysate of cells expressing 3xFLAG-LC3C was used in the LC3L detection experiment. Data from one representative experiment of three independent experiments is presented. LC3A, GFP-LC3A; LC3B, GFP-LC3B; LC3C, GFP-LC3C; RAP, GFP-GABARAP; RAP-L1, GFP-GABARAP-L1; RAP-L2, GFP-GABARAP-L2.

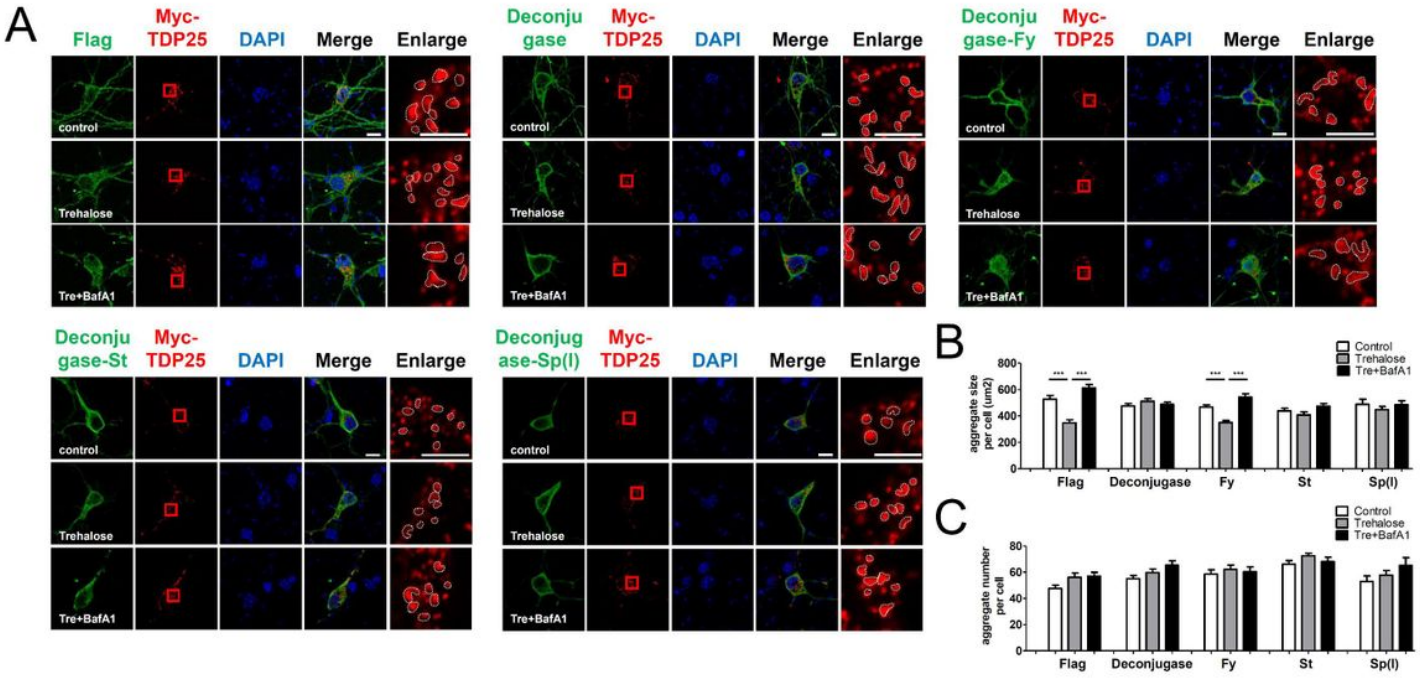

Figure 6

Regulation of TDP25-mediated aggregates by selective mATG8 deconjugases. a, Confocal images showing TDP25-mediated aggregates in mouse cortical neurons expressing Deconjugase-X together with Myc-TDP-25. Scale bar: 10 μm. X: Fy, TP(T), St, 4B(T), or Sp(I). (b-c) Bar graphs show TDP-25 aggregate size (b) or number (c) per cell. Values are presented as means + SEM (n ≥17 for each group). ***P < 0.001.

Supplementary Files

This is a list of supplementary files associated with this preprint. Click to download.

- Supplementalinformation.pdf